

# Theory of Carbon–Sulfur Bond Activation by Small Metal Sulfide Particles

Matthew Neurock\*,† and Rutger A. van Santen

*Contribution from the Schuit Institute of Catalysis, Eindhoven University of Technology, P.O. Box 513, 5600 MB Eindhoven, The Netherlands*

Received August 19, 1993. Revised Manuscript Received December 3, 1993\*

**Abstract:** Elementary reaction steps for the catalytic cycle of thiophene desulfurization on  $\text{Ni}_3\text{S}_2$  and  $\text{Ni}_4\text{S}_4$  clusters are investigated using density functional quantum chemical calculations. The  $\text{Ni}_3\text{S}_2$  cluster is active while the  $\text{Ni}_4\text{S}_4$  cluster is relatively inactive for HDS catalysis. Adsorption and overall reaction energies are computed on complete geometry-optimized cluster–adsorbate systems. The nickel–sulfide cluster is found to significantly reorganize upon interaction with adsorbates. Sulfur readily rearranges between 3-fold and 2-fold binding sites. Hydrogen adsorbs molecularly and dissociates heterolytically over  $\text{Ni}_3\text{S}_2$  to form both adsorbed sulphydryl (SH) and hydral (MH) species. The presence of coadsorbed hydrogen affects both the heat of adsorption and the coordination of thiophene. On the “bare”  $\text{Ni}_3\text{S}_2$  cluster thiophene binds  $\eta^4$ -coordinated, while in the presence of coadsorbed hydrogen thiophene prefers the  $\eta^1$  site. 2,5-Dihydrothiophene (DHT) adsorbs somewhat stronger than thiophene on the  $\text{Ni}_3\text{S}_2$  cluster. In the preferred  $\eta^3$  configuration, the ethylene moiety of the DHT adsorbs at one nickel atom site while its sulfur adsorbs at the neighboring nickel atom site. For the HDS cycles initiated by  $\eta^1$  or  $\eta^4$  thiophene adsorption, the energy change associated with the carbon–sulfur bond scission step of adsorbed dihydrothiophene and that for the removal of sulfur via  $\text{H}_2\text{S}$  are the most endothermic steps and are speculated to be rate limiting. Their comparable values indicate that the two steps compete. The cycle which is initiated by the removal of sulfur from  $\text{Ni}_3\text{S}_2$  is energetically unfavorable.

## Introduction

Small metal sulfide particles are known to be very active heterogeneous hydrodesulfurization catalysts. This was initially demonstrated by de Beer and Prins for sulfidic particles dispersed on high surface area supports.<sup>1–4</sup> Studies using model organometallic clusters supported on carbon and various metal oxides have provided additional evidence for the active role of small clusters in hydrodesulfurization (HDS) chemistry.<sup>5,6</sup> Recently, Welters et al.<sup>7,8</sup> found a direct relationship between HDS activity and the relative number of small particles impregnated in the micropores of zeolite-supported catalysts. Ledoux et al.<sup>9</sup> presented compelling evidence that small metal sulfide clusters not only demonstrate substantial activities (low activation energies) but also follow the same periodic trends as the conventional supported bulk metal sulfides. In light of this similar catalytic behavior, it is expected that the analysis of small transition metal sulfide (TMS) complexes will not only help to discern the chemistry in these clusters but also elucidate insights into possible mechanisms in traditional HDS systems.

The pathways and mechanisms controlling hydrodesulfurization chemistry have been examined, analyzed, and intensely

debated for well over fifty years. Considerable progress has been made by way of deducing important electronic and structural features of the active sites, identifying reaction intermediates, establishing structure–activity relationships, and elucidating governing molecular reaction pathways of HDS. An excellent series of reviews by Topsoe and Clausen,<sup>10</sup> Harris and Chianelli,<sup>11</sup> Prins, de Beer, and Somorjai,<sup>12</sup> and Wiegand and Friend,<sup>13</sup> which discuss the nature of the Co–Mo–S phase, the governing electronic features, the analysis of catalyst structure–function and promoter effects, and the chemistry of model reactants and intermediates on transition metal surfaces and organometallic clusters, respectively, provide a concise summary and a fairly up-to-date report on the chemistry of HDS. While our knowledge base of HDS chemistry has grown substantially, our understanding of the controlling mechanistic steps, however, is still rather poor.

Hydrodesulfurization of the model reactant thiophene has been the target of many previous studies reported in the literature. Subsequently, there have been a number of mechanisms proposed to explain thiophene HDS. Three of the classic mechanisms, discussed in the reviews by Wiegand and Friend<sup>13</sup> and Vissenberg,<sup>14</sup> are Lipsch–Schuit hydrogenolysis,<sup>15</sup> the hydrogenation mechanism, and Kolboe desulfurization.<sup>16</sup> In the Lipsch–Schuit mechanism, the carbon–sulfur bond is directly cleaved due to the presence of hydrogen via hydrogenolysis. In the hydrogenation mechanism, however, the  $\alpha$ -carbon is first hydrogenated prior to carbon–sulfur bond scission. In the final mechanism, which was proposed by Kolboe, the two  $\beta$ -hydrogens are eliminated to form a surface  $\text{H}_2\text{S}$  species with the direct extrusion (desulfurization) of a diacetylene intermediate. The diacetylene is then readsorbed and hydrogenated to yield butadiene.

\* Author to whom correspondence should be sent.

† Present address: DuPont Central Research and Development, Experimental Station, Wilmington, DE 19880-0262.

• Abstract published in *Advance ACS Abstracts*, April 1, 1994.

(1) De Beer, V. H. J.; Duchet, J. C.; Prins, R. J. *Catal.* 1981, 72, 369.  
(2) Duchet, J. C.; van Oers, E. M.; de Beer, V. H. J.; Prins, R. J. *Catal.* 1983, 80, 386.

(3) Vissers, J. P. R.; Groot, C. K.; van Oers, E. M.; de Beer, V. H. J.; Prins, R. *Bull. Soc. Chim. Belg.* 1984, 93, (8), 813.

(4) Vissers, J. P. R.; de Beer, V. H. J.; Prins, R. *J. Chem. Soc., Faraday Trans. 1* 1987, 83, 2145.

(5) Markel, E.; Van Zee, J. W. *J. Mol. Catal.* 1992, 73, 335–351.

(6) Curtis, M. D.; Penner-Hahn, J. E.; Schwank, J.; Baralt, O.; McCabe, D. J.; Thompson, L.; Waldo, G. *Polyhedron* 1988, 7, (22, 23), 2411–2420.

(7) Welters, W. J. J.; Koranyi, T. I.; de Beer, V. H. J.; van Santen, R. A. In *New Frontiers in Catalysis*. Proc. 10th Int. Congr. Catal. Budapest 1992; Guczi, L., Solymosi, F., Tétényi, P., Eds.; Elsevier Science Publishers B.V.: Amsterdam, 1993; pp 1931–1934.

(8) Koranyi, T. I.; van de Ven, L. J. M.; Welters, W. J. J.; de Haan, J. W.; de Beer, V. H. J.; van Santen, R. A. *Catal. Lett.* 1993, 17, 105–116.

(9) Ledoux, M. J.; Michaux, O.; Agostini, G. *J. Catal.* 1986, 102, 275–288.

(10) Topsoe, H.; Clausen, B. S. *Catal. Rev.-Sci. Eng.* 1984, 26, (3, 4), 395–420.

(11) Chianelli, R. R. *Catal. Rev.-Sci. Eng.* 1984, 26, (3, 4), 361–393.

(12) Prins, R.; de Beer, V. H. J.; Somorjai, G. A. *Catal. Rev.-Sci. Eng.* 1989, 31, (1, 2), 1–41.

(13) Wiegand, B. C.; Friend, C. M. *Chem. Rev.* 1992, 92, (4), 491–504.

(14) Vissenberg, M. *Het Mechanisme van de HDS Reaktie*. M.S. Dissertation, University of Amsterdam, 1993.

(15) Lipsch, J. M. J. G.; Schuit, G. C. A. *J. Catal.* 1969, 15, 179.

(16) Kolboe, S. *Can. J. Chem.* 1969, 47, 352.

While the hydrogenation mechanism has the most substantial following, the controlling steps are still under debate. For example, the question of how the energetics of carbon–sulfur bond breaking compare with the energetics for the removal of deposited sulfur is of direct relevance yet still unknown. Classically, the optimal activity has been sited with the optimal metal–sulfide bond strength, as was proposed by Chianelli and Harris.<sup>11,17–20</sup> This is indicative of a competition between two different elementary steps. The first step involves the creation of a surface vacancy by the desorption of H<sub>2</sub>S, whereas the second requires the splitting of the C–S bond in the adsorbed intermediate. Recently, however, Norskov and Topsoe<sup>21</sup> proposed that the optimal catalyst is one which has the weakest metal–sulfur bond strength. They successfully demonstrated the same periodic trends as Chianelli by correlating HDS activity with the bulk sulfur binding energies.

In addition to discerning the rate-controlling step, a number of other more detailed issues pertinent to the mechanism are also unresolved. The first of which concerns the mode of thiophene adsorption. There is ample evidence which demonstrates  $\eta^1(S)$ ,  $\eta^2$ ,  $\eta^4$ ,  $\eta^5$ ,  $\eta^4\text{-S-}\mu_2$ , and  $\eta^4\text{-S-}\mu_3$  binding of thiophene to transition metals in various organometallic complexes.<sup>22</sup> In addition, single-crystal experiments with various transition metals indicate that thiophene adsorbs perpendicular,<sup>12</sup> parallel,<sup>23</sup> and tilted<sup>24,25</sup> to the surface under different conditions. At low coverages thiophene is thought to adsorb parallel (flat) to the surface, whereas at higher coverages thiophene binds either perpendicular or tilted<sup>12,13</sup> through a  $\sigma$ -bond between the sulfur and a metal surface site. The transition from these ideal metal surfaces to active transition metal sulfide catalysts, however, is still unclear and a current topic in the literature.<sup>26–29</sup> Extrapolation from single-crystal results to HDS chemistry, therefore, should be made with appropriate caution.

A second issue regards the binding and dissociation of hydrogen. The traditional hypothesis was that sulphydryl (SH) species are formed via the dissociation of molecular hydrogen and are responsible for carrying out hydrogenation of neighboring thiophene. Recently, Topsoe and Topsoe<sup>30</sup> found from FTIR experiments the presence of these SH groups and discussed their role in HDS activity. A second view concerning hydrogen adsorption indicates that surface hydrol (MH) groups are formed and play an active role in the hydrogenation mechanism. Jobic et al., for example, have recently detected significant amounts of the surface hydrol species through neutron spectroscopy.<sup>31</sup> These species may also be the active precursors for hydrogenation.

A third point associated with the mechanism involves the degree of ring saturation or the number of bonds hydrogenated prior to carbon–sulfur bond scission. Hydrogenation to both the 2,5-dihydrothiophene (DHT) and 2,3,4,5-tetrahydrothiophene (THT) intermediates has been argued. Overall equilibrium suggests that the hydrogenation to THT is favored for temperatures below 623 °C.<sup>32</sup> The kinetic results of Schulz et al.,<sup>33</sup> however, indicate

that the subsequent hydrogenation of DHT to THT competes with the carbon–sulfur bond scission path.

Finally, little is known about the structural changes of the TMS surface due to chemisorption and its influence on the mechanism. Somorjai has shown that surface reconstruction occurs for different transition metals covered with sulfur when CO is introduced, and this can actually alter available paths.<sup>34</sup>

Clearly, additional work aimed at elucidating the mechanism and understanding how structural, electronic, and energetic perturbations affect different reaction paths is required. Small transition metal sulfide clusters, such as those mentioned above for carrying out chemistry on carbon surfaces and within zeolite pores, are of direct practical relevance due to their high HDS activity. In addition, their simplicity makes them valuable probes for the questions raised concerning the mechanisms for HDS.

The finite size of these clusters coupled with their activity at catalytic conditions presents an excellent opportunity to explore hydrodesulfurization mechanisms using first principle quantum chemical calculations. Previous quantum chemical calculations on HDS chemistry modeled the bulk metal sulfide and its active surface with either small TMS clusters or extended surfaces and proved to be invaluable in understanding various aspects of the electronic structure and its relationship to reactivity.<sup>16–20,35–42</sup> For example, Harris and Chianelli<sup>17–20</sup> performed SCF-Xα calculations on MS<sub>6</sub><sup>n-</sup> clusters to relate experimental HDS activities for different first and second row transition metal sulfides with a combination of the metal d contribution to the  $\sigma$ - and  $\pi$ -bonding orbitals and the relative orbital occupation numbers. Norskov, Clausen, and Topsoe<sup>21</sup> demonstrated a similar comparison to HDS activity with ab initio computed sulfur-binding energies for both first and second row bulk transition metal sulfides. Anderson et al.<sup>35,36</sup> used the atomic superposition and electron delocalization (ASED) method, to look at methane conversion, Fischer–Tropsch catalysis over fixed MoS<sub>2</sub> clusters. Diez and Jubert<sup>37</sup> studied the adsorption of hydrogen and the removal of sulfur from model MoS<sub>2</sub> clusters using extended Hückel calculations. Rong et al.<sup>38,39</sup> used molybdenum, cobalt, and ruthenium sulfide clusters and DV-Xα calculations to model bulk MoS<sub>2</sub>, Co<sub>9</sub>S<sub>8</sub>, and RuS<sub>2</sub>. Adsorption was studied by bringing in adsorbates at various sites and analyzing changes in bond orders and atomic charges. Zonneville, Hoffmann, and Harris<sup>40</sup> provided a detailed account of the MoS<sub>2</sub> surface, the adsorption of thiophene, the role of defect sites, promoters and poisons, and a number of other relevant issues through infinite slab extended Hückel calculations. Rouette et al.<sup>41</sup> outlined an in-depth orbital analysis of thiophene adsorption on Mo(CO)<sub>3</sub> and Mo(CO)<sub>5</sub> clusters using semiempirical CNDO-UHF calculations. Rodriguez<sup>42</sup> analyzed the bonding of thiophene, sulphydryl, thiomethoxy, and phenyl thiolate on Mo surfaces with semiempirical INDO calculations.

While each of these studies provided useful information toward the qualitative understanding of hydrodesulfurization, the absence of complete geometry optimization and/or limitations in the methods used precluded any quantitative energetics. The work by Norskov et al.,<sup>21</sup> where advanced ab initio techniques were employed to describe the TMS system, however is a definite exception.

With the recent (5–10 years) developments in both theoretical methods and computational resources, reasonable estimates for

- (17) Harris, S. *Chem. Phys.* **1982**, *67*, 229.
- (18) Harris, S.; Chianelli, R. R. *Chem. Phys. Lett.* **1983**, *101*, 603–605.
- (19) Harris, S.; Chianelli, R. R. *J. Catal.* **1984**, *86*, 400–412.
- (20) Harris, S.; Chianelli, R. R. *J. Catal.* **1986**, *98*, 17–31.
- (21) Norskov, J. K.; Clausen, B. S.; Topsoe, H. *Catal. Lett.* **1992**, *13*, 1–8.
- (22) Angelici, R. J. *Coord. Chem. Rev.* **1990**, *105*, 61–76.
- (23) Netzer, F. P.; Bertel, E.; Goldmann, A. *Surf. Sci.* **1988**, *201*, 257.
- (24) Fulmer, J. P.; Zaera, F.; Tysoe, W. T. *J. Phys. Chem.* **1988**, *92*, 4147.
- (25) Stohr, J.; Gland, J. L.; Kollin, E. B., et al. *Phys. Rev. Lett.* **1984**, *53*, 2161.
- (26) Xu, H.; Friend, C. M. *J. Phys. Chem.*, in press.
- (27) Xu, H.; Uvdal, P.; Friend, C. M.; Stohr, J. *Surf. Sci.*, in press.
- (28) Roberts, J. T.; Friend, C. M. *Surf. Sci.* **1987**, *186*, 201.
- (29) Gellman, A. J.; Neiman, D.; Somorjai, G. A. *J. Catal.* **1987**, *107*, 92–113.
- (30) Topsoe, N.; Topsoe, H. *J. Catal.* **1993**, *139*, 641–651.
- (31) Jobic, H.; Clugnet, G.; Lacroix, M.; Yuan, S.; Mirodatos, C.; Breysse, M. *J. Am. Chem. Soc.*, in press.
- (32) Weisser, O.; Landa, S. *Sulphide Catalysts, Their Properties and Applications*; Pergamon Press: Oxford, 1973.
- (33) Schuz, H.; Schon, M.; Rahman, N. *Catalytic Hydrogenations*, Cerveny, L., Ed.; Elsevier: Amsterdam, 1986; pp 201–255.

- (34) Somorjai, G. A. In *Elementary Reaction Steps in Heterogeneous Catalysis*; Joyner, R. W., van Santen, R. A., Eds.; NATO ASI Series 398; Kluwer Academic Publ.: Dordrecht, 1993; pp 3–39.
- (35) Anderson, A. B.; Maloney, J. J.; Yu, J. *J. J. Catal.* **1988**, *112*, 392–400.
- (36) Anderson, A. B.; Yu, J. *J. J. Catal.* **1989**, *119*, 135–145.
- (37) Diez, R. P.; Jubert, A. H. *J. Mol. Catal.* **1992**, *73*, 65–76.
- (38) Rong, C.; Qin, X. *J. Mol. Catal.* **1991**, *64*, 321–335.
- (39) Rong, C.; Qin, X.; Jinglong, H. *J. Mol. Catal.* **1992**, *75*, 253–276.
- (40) Zonneville, M. C.; Hoffmann, R.; Harris, S. *Surf. Sci.* **1988**, *199*, 320.
- (41) Rouette, F.; Valencia, N.; Sanchez-Delgado, R. *J. Am. Chem. Soc.* **1989**, *111*, 40–46.
- (42) Rodriguez, J. *Surf. Sci.* **1992**, *278*, 326–338.

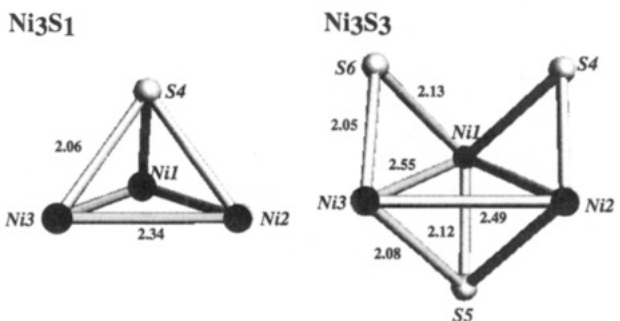
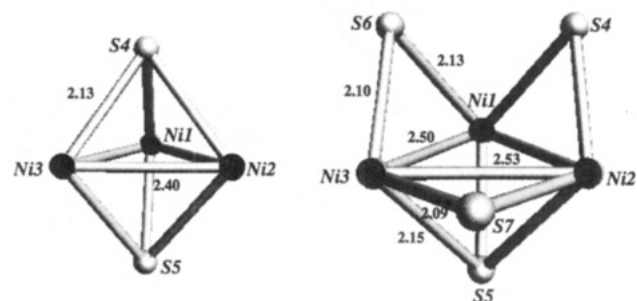
the energetics and bonding in transition metal and transition metal sulfide systems are now possible. Density functional theory, for example, has advanced to the stage where it can predict valuable information on transition metal systems. Ziegler<sup>43</sup> published an excellent review on different DFT-based methods and their accuracy in predicting structure (bond lengths, bond angles, and torsion angles), bond energies, potential energy surfaces, transition-state structures, reaction paths, vibrational frequencies, force fields, ionization potentials, excitation energies, and electron affinities. Structural calculations are good to within 0.01 Å for bonds and 1–2° for bond angles and torsion angles. Bond energies for clusters containing transition metal atoms are good to within 20 kJ/mol. More recent estimates for general systems show bond energies to be within about 10 kJ/mol.<sup>44,45</sup>

In this paper, we exploit both the attractiveness of the finite size of the active metal sulfide particles and the advances in theoretical methods, by exploring elementary HDS pathways on small  $\text{Ni}_x\text{S}_y$  clusters with density functional quantum chemical techniques. We focus on elucidating the structural, electronic, and energetic effects for the interaction of atomic sulfur (S), molecular hydrogen ( $\text{H}_2$ ), hydrogen sulfide ( $\text{H}_2\text{S}$ ), thiophene (TH), and 2,5-dihydrothiophene (DHT) with  $\text{Ni}_3\text{S}_y$  and  $\text{Ni}_4\text{S}_y$  clusters. We probe the energetics of different binding sites, adsorbate-induced structural reorganizations, and the effects of coadsorption. With regard to the mechanism, we scrutinize both  $\eta^1$ - and  $\eta^4$ -thiophene adsorption-mediated pathways in an attempt to uncover overall reaction energies and rate-limiting steps for each path. In addition, we study the energetic effects due to the relative ordering of adsorption steps in the overall cycle. Finally, we attempt to determine whether it is the intermediate adsorbed sulfur or lattice sulfur which serves as the precursor to HDS catalysis by comparing the reaction pathway energetics for two competing cycles. In the former, sulfur is added by way of thiophene adsorption, while in the later a single sulfur atom is removed from the cluster to initiate the cycle.

## Methods

The density functional calculations reported in this work were completed using the DGauss program by Cray Research Inc.<sup>46</sup> As in most density functional algorithms, a set of single-particle Kohn-Sham equations are solved self-consistently where electron-electron interactions are embodied in the exchange-correlation potential term of the Hamiltonian. The local spin density approximation (LSD) is invoked to provide a computational means of estimating the exchange-correlation potential. The DGauss program implements the analytical form of the LDA potential proposed by Vosko, Wilk, and Nusair.<sup>47</sup> Nonlocal gradient corrections to both the exchange and correlation energies are provided subsequent to the SCF solution. The form of the exchange and correlation energy corrections is taken from Becke<sup>48,49</sup> and Perdew,<sup>50</sup> respectively. All calculations reported here were done using the “all-electron” approach, where the coefficients for both the valence as well as the core orbitals are varied in the SCF. Optimized Gaussian basis functions were used, which result in reasonably accurate determinations of reaction energetics. Energy gradients are evaluated analytically and therefore allow for expedient geometry optimizations. All geometry optimizations were performed at the LSD level. Nonlocal corrections were included for each of the final optimized structures. More on the basis sets, fit sets, and convergence criterion used in the calculations and the overall algorithm are presented in the supplementary material.

The clusters used in this work were chosen to represent different electronic and structural models for the NiS system. The relative size of the active nickel sulfide particles impregnated inside the pores of a zeolite has been estimated to be composed of five or fewer nickel atoms.<sup>7</sup>

Ni<sub>3</sub>S<sub>2</sub>Ni<sub>3</sub>S<sub>4</sub>Ni<sub>3</sub>S<sub>1</sub>Ni<sub>3</sub>S<sub>3</sub>Figure 1. Optimized structures of  $\text{Ni}_3\text{S}_y$ .

Therefore, we chose the neutral  $\text{Ni}_3\text{S}_x$  and the  $\text{Ni}_4\text{S}_y$  clusters for our calculations to mimic these systems. In addition, these clusters provide an informative range of different formal nickel oxidation states with minimal computational burden.

## Results and Discussion

The results herein are discussed in terms of the structural, electronic, and energetic changes due to (1) addition and removal of atomic sulfur, (2) molecular and dissociative adsorption of hydrogen and hydrogen sulfide, (3) the adsorption of thiophene and 2,5-dihydrothiophene, and (4) coadsorption and hydrogenation on the  $\text{Ni}_3\text{S}_x$  and  $\text{Ni}_4\text{S}_x$  clusters. This information is subsequently used to compute and compare the energetics of elementary reaction steps for different postulated catalytic HDS cycles.

**I. Interaction of Atomic Sulfur with  $\text{Ni}_4\text{S}_x$  and  $\text{Ni}_3\text{S}_x$ . Structural Rearrangements.** The structural changes involved in the sequential addition of sulfur were explored by performing full geometry optimizations on the following two series:  $\text{Ni}_3\text{S}_1$ ,  $\text{Ni}_3\text{S}_2$ ,  $\text{Ni}_3\text{S}_3$ , and  $\text{Ni}_3\text{S}_4$ , and  $\text{Ni}_4\text{S}_3$ ,  $\text{Ni}_4\text{S}_4$ , and  $\text{Ni}_4\text{S}_5$ . The resulting optimized geometries are depicted in Figures 1 and 2. Due to the lack of symmetry operations and known numerical gradient fluctuations for DFT calculations,<sup>51</sup> the values reported in Figure 1 and the remainder of this work were determined within  $\pm 0.01$  Å. It is evident from these figures that sulfur prefers the higher 3-fold coordination sites, as witnessed for the addition of S to both  $\text{Ni}_3\text{S}_1$  and  $\text{Ni}_4\text{S}_3$  to form  $\text{Ni}_3\text{S}_2$  and  $\text{Ni}_4\text{S}_4$ . When 3-fold binding sites are unavailable, the sulfur assumes the 2-fold bridge sites, as shown for the addition of sulfur to  $\text{Ni}_3\text{S}_2$ ,  $\text{Ni}_3\text{S}_3$ , and  $\text{Ni}_4\text{S}_4$ . The optimized addition of sulfur to  $\text{Ni}_3\text{S}_2$  demonstrates an interesting structural reorganization. Sulfur 4 (in  $\text{Ni}_3\text{S}_2$  of Figure 1), which is initially situated at a 3-fold pyramidal-capping site, migrates to a 2-fold position. The optimized  $\text{Ni}_3\text{S}_3$  cluster now contains two 2-fold-bound sulfurs rather than one 3-fold and one 2-fold sulfur atoms. This can be described in terms of the principle of least metal atom sharing<sup>52</sup> and is consistent with Shustorovich's bond order conservation (BOC) principle.<sup>53,54</sup> According to the

(43) Ziegler, T. *Chem. Rev.* **1991**, *91*, 651.  
 (44) Becke, A. D. *J. Chem. Phys.* **1993**, *98*, 2, 1372.  
 (45) Johnson, B. G.; Gill, P. M. W.; Pople, J. J. *J. Chem. Phys.* **1993**, *98*, 7, 5612.

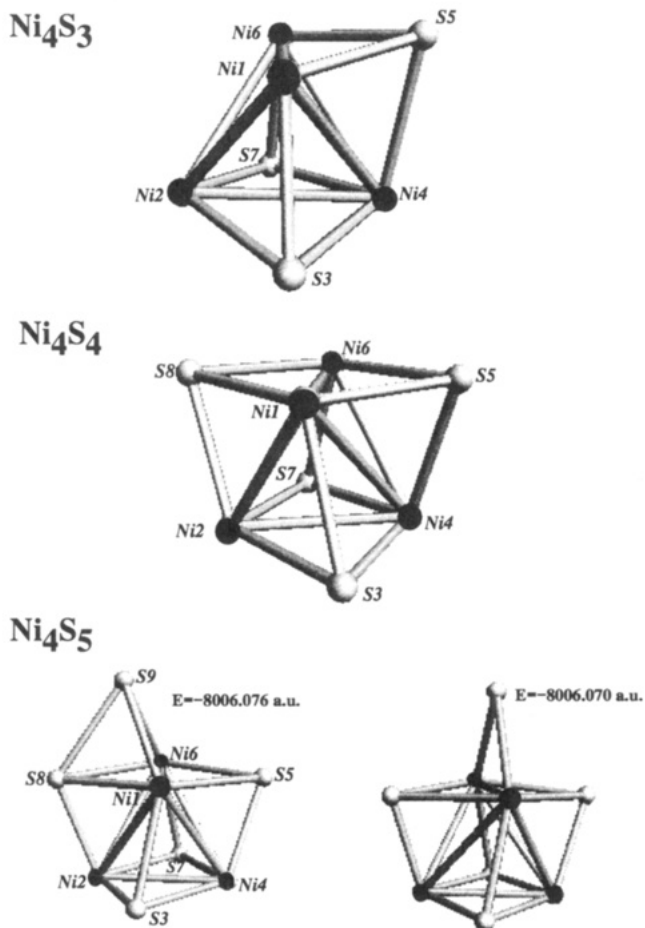
(46) Andzelm, J.; Wimmer, E. *J. Chem. Phys.* **1992**, *96*, (2), 1280–1303.  
 (47) Vosko, S. H.; Wilk, L.; Nusair, M. *Can. J. Phys.* **1980**, *58*, 1200.  
 (48) Becke, A. D. *Phys. Rev. A* **1988**, *38*, 3098.  
 (49) Becke, A. *ACS Symp. Ser.* **1989**, *394*, 165.  
 (50) Perdew, J. P. *Phys. Rev. B* **1986**, *33*, 8822.

(51) Sosa, C.; Andzelm, J.; Elkin, B. C.; Wimmer, E.; Dobbs, K.; Dixon, D. A. *J. Phys. Chem.* **1992**, *96*, 6630.

(52) Van Santen, R.; Zonnevylle, M. C.; Jansen, A. P. *J. Philos. Trans. R. Soc. London, A* **1992**, *341*, 269–282.

(53) Shustorovich, E. *Surf. Sci. Rep.* **1986**, *6*, 1.

(54) Shustorovich, E. *Adv. Catal.* **1990**, *37*, 101.

Figure 2. Optimized structures of  $\text{Ni}_4\text{S}_x$ .

BOC principle, the reactivity of an atom decreases with increasing coordination number. In the optimized  $\text{Ni}_3\text{S}_3$  cluster, the two bridge sulfurs share only a single nickel atom, whereas in the alternative situation (one 3-fold and one 2-fold) the two sulfurs share two nickel atoms. The former is energetically much more favorable. The subsequent binding of an additional sulfur on  $\text{Ni}_3\text{S}_3$  to form  $\text{Ni}_3\text{S}_4$  has little to gain by structural reorganization and therefore bonds to the vacant bridge site, as is shown in the final structure in Figure 1. The preference for 3-fold coordination of atomic sulfur at low Ni/S ratios is consistent with available literature on bare transition metal clusters and surfaces, which indicates that sulfur,<sup>55,56</sup> as well as atomic oxygen,<sup>57,58</sup> hydrogen,<sup>55,59,60</sup> and carbon,<sup>61</sup> prefers higher fold coordination sites. The interaction between the hydrogen 1s and the oxygen, sulfur, and carbon 2p orbitals with surface metal d orbitals tends to dominate the bonding.

Table 1 presents the average changes in the Ni–Ni and Ni–S bond lengths due to the addition of sulfur. The results demonstrate that the Ni–Ni distance elongates upon the sequential addition of sulfur. Specific changes in the individual bond lengths were shown in Figure 1. The addition of sulfur to  $\text{Ni}_3\text{S}_1$  to form  $\text{Ni}_3\text{S}_2$  creates three new Ni–S bonds, one to each nickel atom, thus weakening the bonds between these Ni atoms and their nearest

(55) Upton, T.; Goddard, W. A., III. *Critical Reviews in Solid State and Materials Science*; CRC: Boca Raton, FL, 1981, 261.

(56) Chesters, M. A.; Lennon, D.; Ackermann, L.; Haberlen, O.; Kruger, S.; Rosch, N. *Surf. Sci.* 1993, 291, 177.

(57) Siegbahn, P. E.; Wahlgren, U. *Int. J. Quantum Chem.* 1992, 42, 1149.

(58) Fournier, R.; Salahub, D. R. *Surf. Sci.* 1991, 245, 263.

(59) Siegbahn, P. E. M.; Blomberg, M. R. A.; Bauschlicher, C. W., Jr. *J. Chem. Phys.* 1984, 81, 4, 2103.

(60) Ellis, D. E.; Cheng, J. P. *Advances in Quantum Chemistry*; Academic Press: New York, 1991; Vol. 22, p 125.

(61) Fournier, R.; Andzelm, J.; Goursot, A.; Russo, N.; Salahub, D. R. *J. Chem. Phys.* 1990, 93, 4.

**Table 1.** Averaged Metal–Metal and Metal–Sulfur Bond Lengths in  $\text{Ni}_3\text{S}_y$  and  $\text{Ni}_4\text{S}_y$  Geometry-Optimized Clusters

cluster	averaged bond lengths (Å)	
	Ni–Ni	Ni–S
$\text{Ni}_3\text{S}_1$	2.34	2.06
$\text{Ni}_3\text{S}_2$	2.40	2.13
$\text{Ni}_3\text{S}_3$	2.52	2.06/2.13
$\text{Ni}_3\text{S}_4$	2.52	2.10/2.14
$\text{Ni}_4\text{S}_3$	2.51	2.11
$\text{Ni}_4\text{S}_4$	2.48/2.81	2.14
$\text{Ni}_4\text{S}_5$	2.61	2.17

neighbors. This is illustrated by the increase in the metal–metal and metal–sulfur bond lengths on going from  $\text{Ni}_3\text{S}_1$  to  $\text{Ni}_3\text{S}_2$ . The further addition of sulfur to the cluster to form  $\text{Ni}_3\text{S}_3$  has a complex effect. Ni1 increases in coordination from 4 to 5, whereas Ni2 and Ni3 retain coordination numbers of 4. This in turn weakens all bonds to Ni1, which explains the longer Ni1–Ni3, Ni1–Ni2, and Ni1–S4, Ni1–S6 bond lengths. As a direct consequence of the weaker Ni1–Ni2 and Ni1–Ni3 bonds (from the BOC principle), the remaining bonds from Ni2 and Ni3 now become slightly stronger. This explains the shorter distance between Ni2 and Ni3, as well as the shorter Ni3–S6, Ni3–S5, Ni2–S4, and Ni2–S5 bond lengths. The final addition of sulfur to the cluster to create  $\text{Ni}_3\text{S}_4$  was also found to bind at a 2-fold coordination site. The coordination of Ni2 and Ni3 are now also increased to 5. Hence, the bonds associated with each of these atoms are slightly increased in length, as is depicted in both Figure 1 and Table 1. The average Ni–S bonds appear to be in good agreement with the value of 2.15 Å for the high sulfur coordination sites reported by Upton and Goddard.<sup>55</sup>

A similar analysis of the structural changes in the  $\text{Ni}_4\text{S}_y$  clusters was also performed. Overall geometric changes are depicted graphically in Figure 2, whereas the accompanying changes in average bond lengths are tabulated in Table 1. Structural optimization for the  $\text{Ni}_4\text{S}_4$  cluster (the middle portion of Figure 2) found that this system was more stable in a cubane type arrangement rather than a cubic salt-structure. In the cubane cluster, the four nickel atoms form an inner tetrahedron, while the four sulfur atoms cap the four faces of this tetrahedron. These sulfur atoms thus form an outer tetrahedron structure. These are not true tetrahedrons in that the six metal–metal (or sulfur–sulfur) distances are not identical. This is most notable in the nickel “tetrahedron”, where two of the Ni–Ni bonds are substantially longer (2.81 Å) than the remaining four (2.48 Å). Harris<sup>62</sup> presented an interesting review on the bonding in metal sulfide cubane clusters and discussed that both the fragment orbital symmetry and the metal electron count are responsible for the distortion of a cubane from pure tetrahedral symmetry. Based on the core valence electron approach,<sup>62–65</sup> our  $\text{Ni}_4\text{S}_4$  cluster has a total of 56 valence electrons (eight d metal electrons). We are four electrons short of the 60 electrons (12 d metal electrons) required for occupation of all valence bonding orbitals. This incomplete occupation of bonding orbitals ultimately leads to the two elongated Ni–Ni bonds. Returning to Table 1, both the Ni–Ni and the Ni–S distances are, in general, increased upon the addition of sulfur to the  $\text{Ni}_4\text{S}_x$  cluster ( $x = 3–5$ ), thus indicating a weakening of both types of bonds. One interesting feature displayed at the bottom of Figure 2 is that the addition of sulfur to  $\text{Ni}_4\text{S}_4$  in a symmetric 2-fold position is close in energy to the “quasi” 3-fold Ni–Ni–S site. This suggests that there may be some small influence due to sulfur–sulfur bonding in systems with excess sulfur contents.

**Electronic Structure.** The changes in the electronic structure induced by the addition of sulfur to the  $\text{Ni}_3\text{S}_y$  and  $\text{Ni}_4\text{S}_y$  clusters

(62) Harris, S. *Polyhedron* 1989, 8, (24), 2843–2882.

(63) Lauher, J. W. *J. Am. Chem. Soc.* 1978, 100, 5305.

(64) Nelson, L. L.; Lo, F. Y. K.; Rae, A. D.; Dahl, L. F. *J. Organomet. Chem.* 1982, 225, 309.

(65) Simon, G. L.; Dahl, L. F. *J. Am. Chem. Soc.* 1973, 95, 2164.

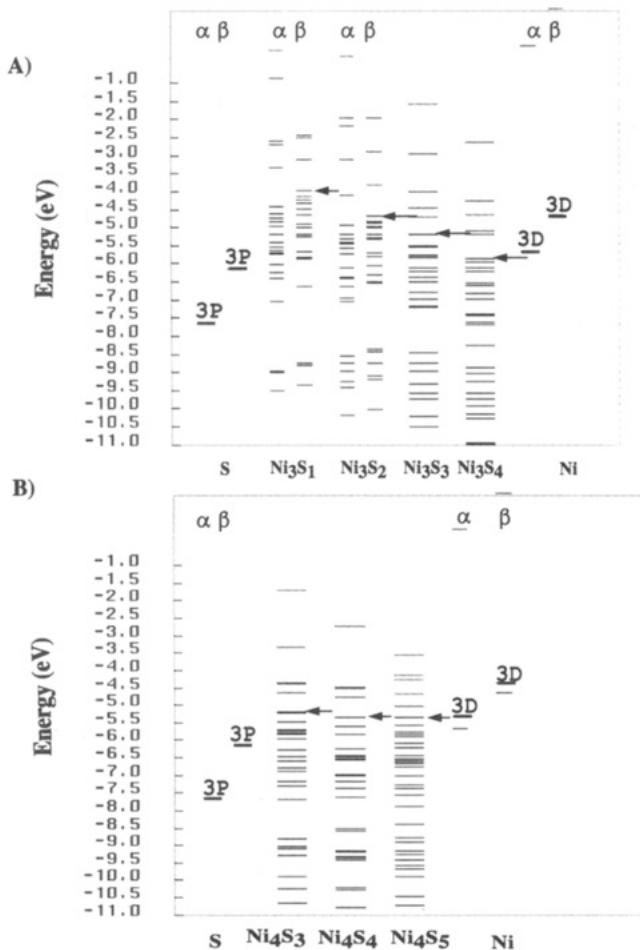


**Figure 3.** Orbital energy spectra for the eigenvalues closest to the highest and lowest MOs for the  $\text{Ni}_3\text{S}_y$  and  $\text{Ni}_4\text{S}_y$  clusters.

are illustrated in the molecular orbital energy spectra depicted in Figure 3. Only the orbitals closest to the HOMO-LUMO gap and those available for adsorbate binding are shown (between 0 and -11 eV). The highest occupied orbital in each cluster is indicated by the arrow. Figure 3, part A, compares the eigenvalue spectra for the three  $\text{Ni}_3\text{S}_y$  clusters and the spectra of the base atomic sulfur and nickel orbitals. Sulfur, nickel,  $\text{Ni}_3\text{S}_1$ , and  $\text{Ni}_3\text{S}_2$  each have open-shell configurations, and therefore, both alpha ( $\alpha$ ) and beta ( $\beta$ ) spins are illustrated. The lowest energy states of  $\text{Ni}_3\text{S}_3$  and  $\text{Ni}_4\text{S}_4$ , however, have closed-shell configurations, and therefore, only closed-shell representations are illustrated. This is denoted by the slightly longer lines for the eigenvalues in these systems. The eigenstates closest to the HOMO-LUMO gap are derived from the interaction of the atomic 3p S orbitals (with eigenvalues of  $\alpha = -7.65$  eV and  $\beta = -6.13$  eV) and the 3d Ni orbitals ( $\alpha = -5.66$  eV and  $\beta = -4.64$  eV). This S-p and Ni-d orbital overlap is consistent with the literature findings for oxygen<sup>57,58</sup> and sulfur<sup>55</sup> on bare nickel clusters. These interactions are more clearly depicted in the orbital illustrations in Figure 4 for many of these states. Just below these metal-sulfur states are a set of MOs composed of combinations of metal d orbital interactions. The nickel s atomic orbitals are found to be pushed upward and take part in the MOs just above the LUMO. The net effect of adding sulfur to both the  $\text{Ni}_3\text{S}_y$  and  $\text{Ni}_4\text{S}_y$  series, as displayed in the orbital energy plots in Figure 3, was to lower the HOMO, which is reflected in the increased binding energy.

**Energetics.** The total energies for all atoms, molecules, clusters, and adsorbate-cluster complexes studied in this work are summarized in Table 2. Both the local spin density derived total energies,  $E_{\text{LSD}}$ , and the total energies which include Becke and Perdew nonlocal corrections,  $E_{\text{NLSD}}$ , are reported in this table.

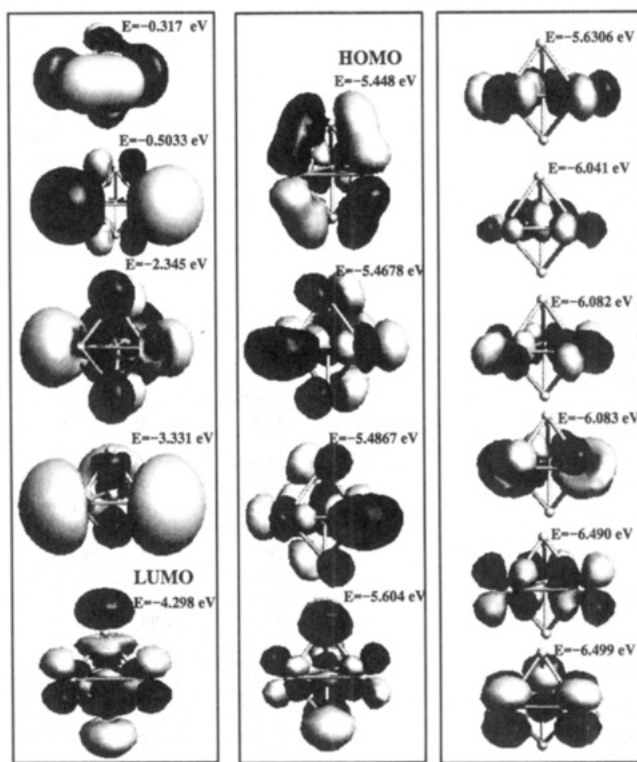


**Figure 4.** Molecular orbitals closest to the highest and lowest occupied orbital for the  $\text{Ni}_3\text{S}_2$  cluster.

All subsequent energetic analyses are based on the gradient-corrected energies ( $E_{\text{NLSD}}$ ). The results in this table follow in the order of atoms, molecules, clusters, and adsorbate-cluster systems. In addition, the energies for various spin states are reported. In general, higher spin states were computed when an orbital analysis indicated that a change in the spin arrangement would result in a lower energy state.

Both atomic binding energies and molecular adsorption energies were computed via eq 1. The adsorption energy is defined here

$$\Delta E_{\text{ADS}} = E_{\text{Ni}_x\text{S}_y+\text{Ads}} - E_{\text{Ni}_x\text{S}_y} - E_{\text{Ads}} \quad (1)$$

as the difference in energy between the combined adsorbate- $\text{Ni}_x\text{S}_y$  cluster system ( $E_{\text{Ni}_x\text{S}_y+\text{Ads}}$ ) and the energy of the free  $\text{Ni}_x\text{S}_y$  cluster ( $E_{\text{Ni}_x\text{S}_y}$ ) and the free gas-phase adsorbate ( $E_{\text{Ads}}$ ). Binding energies are defined similarly with the exception that the adsorbate now refers to the atomic adatom. The actual values used to compute adsorption/binding energies are the nonlocally corrected total energies ( $E_{\text{NLSD}}$ ) summarized in Table 2. Each of these energies was derived from full geometry optimizations and thus reflect any structural changes in the adsorbate or cluster induced by adsorption. The adsorption energies derived in this work strictly include energy costs associated with changes in electronic state, such as singlet to triplet. These are actual requirements for *real clusters*, such as the models analyzed in this work. For systems which employ clusters to model a *transition metal surface*, however, this energy cost is an artifact of using finite clusters with measurable energetic differences between the HOMO and LUMO to model an infinite surface with a continuous band. Seigbahn and Wahlgren<sup>57</sup> provide an nice discussion on this effect for bare transition metal surfaces and the application of the bond preparation method.

**I. Sulfur Binding.** The binding energies for sulfur to the  $\text{Ni}_3\text{S}_y$  and  $\text{Ni}_4\text{S}_y$  cluster series are shown in the first part of Table 3. The addition of sulfur to each of the clusters was found to be highly exothermic. Consequently, the reverse reaction, sulfur removal, is highly endothermic. The following order exists:



**Table 2.** Total LSD and NLSD Energies for the Atoms, Organics, Metal Sulfides, and Adsorbate/Metal-Sulfide Species

components	$E_{LSD}$ (hartree)	$E_{NLSD}$ (hartree)
Atoms		
hydrogen (sing.)	-0.476 526 37	-0.498 126 880
carbon (sing.)	-37.463 311 995	-37.774 949 49
carbon (trip.)	-37.464 370 55	-37.838 985 20
sulfur (sing.)	-396.684 574 1339	-398.071 374 86
sulfur (trip.)	-396.679 581 37	-398.102 749 42
nickel (trip.)	-1505.318 504 56	-1508.241 842 83
Organic Compounds		
$H_2$	-1.136 855 70	-1.176 355 06
$H_2S$	-397.952 492 79	-399.395 1041
cis-butadiene	-154.538 635 60	-156.008 440
trans-butadiene		-152.711 4232
thiophene	-550.212 979 16	-553.042 400 34
2,5-dihydrothiophene	-551.381 5075	-554.239 893 05
Metal Sulfide Clusters		
$Ni_1S_1$ (sing.)	-1902.144 1710	-1906.457 103 988
(trip.)	-1902.181 917 50	-1906.504 610 750
$Ni_3S_1$ (sing.)	-4913.086 909 97	-4923.188 977 91
(trip.)	-4913.129 643 21	-4923.228 420 18
(quin.)	-4913.074 435 76	-4923.189 495 54
$Ni_3S_2$ (sing.)	-5309.980 3331	-5321.465 031 98
(trip.)	-5310.024 272 34	-5321.505 809 56
(quin.)	-5309.975 249 63	-5321.453 792 31
$Ni_3S_3$ (sing.)	-5706.880 505 42	-5719.757 277 00
(trip.)	-5706.866 304 92	-5719.743 707 76
$Ni_3S_4$ (sing.)	-6103.733 607 06	-6117.944 969 93
$Ni_4S_3$ (sing.)	-7212.385 407 76	-7228.144 391 94
$Ni_4S_4$ (sing.)	-7609.254 657 47	-7626.398 552 70
$Ni_4S_5$ (sing.)	-8006.675 907 19	-8024.604 071 97
Adsorbate/Metal Sulfide		
$Ni_3S_1-H_2$ (homo)	-4914.302 233 99	-4924.420 955 34
$Ni_3S_1-2H$ (homo)	-4914.306 148 99	-4924.424 404 072
$Ni_3S_1-SH-H$ (H 2-fold)	-5311.183 583 97	-5322.693 851 52
$Ni_3S_1-2H-\eta^1\text{-thiophene}$ (sing.)	-5464.557 2840	-5477.495 448 29
(trip.)	-5464.564 3511	-5477.484 976 22
$Ni_3S_1-\eta^1\text{-DHT}$ (trip.)	-5464.579 602 39	-5477.510 396 74
$Ni_3S_1-SH-H-\eta^4\text{-DHT}$		-5875.773 193 57
$Ni_3S_2-H$ 1-fold (Ni)	-5310.576	-5322.072 471 65
2-fold (Ni)	-5310.604 358 37	-5322.100 971 65
3-fold (Ni)	-5310.585 216 16	-5322.081 199 28
$Ni_3S_2-H_2$ (homo) (sing.)	-5311.190 509 77	-5322.705 841 61
$Ni_3S_2-2H$ (homo) (sing.)	-5311.183 159 41	-5322.691 258 24
$Ni_3S_2-2H$ (hetero) (sing.)	-5311.157 083 67	-5322.670 476 12
(hetero) (trip.)	-5311.161 877 77	-5322.675 583 72
$Ni_3S_2-2H$ (hetero) (H 2-fold)	-5311.183 583 97	-5322.693 851 52
$Ni_3S_2-H_2S$	-5708.017 349 71	-5720.938 102 50
$Ni_3S_2-H-SH$	-5708.011 390 88	-5720.919 158 88
$Ni_3S_2-H-SH$ (both 2-fold)	-5798.028 201 30	-5720.928 637 86
$Ni_3S_2-\eta^1\text{-thiophene}$ (sing.)	-5860.288 568 64	-5874.580 278 96
$Ni_3S_2-\eta^4\text{-thiophene}$ (sing.)	-5860.3287	-5874.600 449 98
$Ni_3S_2-\eta^1\text{-thiophene}-2H$ (sing.)	-5861.453 135 26	-5875.761 765 57
(trip.)	-5861.444 1811	-5875.746 689 46
$Ni_3S_2-\eta^4\text{-thiophene}-2H$		-5875.758 934 33
$Ni_3S_2-\eta^1\text{-thiophene}-H$	-5860.878 169 96	-5875.175 653 34
$Ni_3S_2-\eta^1\text{-DHT}$	-5861.472 056 00	-5875.792 382 04
$Ni_3S_2-\eta^4\text{-DHT}$	-5861.510 520 15	-5875.806 572 28
$Ni_3S_2$ -hydrothiophene	-5860.855 623 63	-5875.155 601 36
$Ni_4S_4-H_2$		
$Ni_4S_4-2H$	-7610.330 896 48	-7627.487 109 32
$Ni_4S_4-H_2S$	-8007.205 022 45	-8025.771 350 54
$Ni_4S_4$ -thiophene		-8179.411 611 77

For either series,  $Ni_3S_y$  or  $Ni_4S_y$ , the energy liberated upon addition of atomic sulfur appears to increase with increasing Ni/S ratio, as expected from the BOC principle. The subsequent addition of new sulfur atoms tends to weaken the overall binding energy. These results are in line with the changes in the average bond lengths upon sulfur addition.

The binding energy of sulfur can also be expressed on a per bond basis. This may be more insightful in understanding the bonding and relative changes in bonding due to structural reorganization. These energies directly account for changes in coordination number. They also provide a means for comparison with estimates of bulk metal sulfide bond energies computed from

available heat of formation data. For bulk NiS, the total energy of formation was estimated from tabulated thermochemical information.<sup>66</sup> The resulting energy was subsequently divided by the total number of Ni–S bonds per Ni atom to estimate an average bulk Ni–S bond energy of +116 kJ/mol. This value is reported in Table 4 along with computed Ni–S bond energies for  $Ni_3S_2$ ,  $Ni_3S_3$ ,  $Ni_3S_4$ ,  $Ni_4S_4$ , and  $Ni_4S_5$  clusters. These cluster bond energies were calculated by dividing the total sulfur binding energy (from Table 3) by the number of Ni–S bonds broken per sulfur atom removed. For example, the removal of the 2-fold sulfur from  $Ni_3S_3$  costs +391 kJ/mol, thus the bond energy is estimated as 391/2 or +196 kJ/(mol Ni–S bond). The results in Table 4 indicate that the bond energies for the  $Ni_3S_y$  clusters are somewhat lower and more closely resemble the bulk situation. This is most likely due to the higher Ni atom coordination numbers. The variation in Ni–S bond energy with composition and cluster size also demonstrates the importance of electronic relaxation effects. An approach based on simple bond additivity would not have been able to accurately deduce these values.

**II. Adsorption of  $H_2$ ,  $H_2S$ , Thiophene, and Dihydrothiophene on  $Ni_3S_y$  and  $Ni_4S_y$  Clusters.** The adsorption of hydrogen, hydrogen sulfide, thiophene, and 2,5-dihydrothiophene on both the  $Ni_3S_2$  and  $Ni_4S_4$  clusters was examined by optimizing the adsorbate–cluster system. In some instances adsorbates were found to bind favorably at various coordination sites, and therefore, different starting geometries were investigated to identify each of these stable structures. All computed adsorption energies are tabulated in Table 3.

In a cursory effort to deduce the most favorable sites on these clusters for the dissociative addition of hydrogen, atomic hydrogen was adsorbed at 1-, 2-, and 3-fold coordination sites on  $Ni_3S_2$ . Figure 5, part A, depicts the optimized binding at each of these sites along with the associated adsorption energies. Clearly, atomic hydrogen binds at all three sites. The most favorable position is the unsaturated 2-fold metal atom site, as was also the case for the binding of additional atomic sulfur. Hydrogen binding at the higher coordination sites is consistent with the work in the literature on bare nickel clusters.<sup>55,59</sup>

Molecular and dissociative adsorption of hydrogen on the series of  $Ni_3S_y$  clusters was also analyzed. The results are depicted in Figure 5, parts B–D. On the  $Ni_3S_2$  cluster, molecular adsorption was favored (-62 kJ/mol), followed by the heterolytic dissociation of hydrogen (-31 kJ/mol) to form the sulphydryl (SH) group and the hydride (H), both of which bind at 2-fold metal coordination sites. The homolytic dissociation of hydrogen to form two 2-fold-coordinated hydrides (-23 kJ/mol) was only slightly less favorable than heterolytic cleavage. Finally, heterolytic dissociative adsorption to produce the 2-fold SH and a singly coordinated hydride was found to be unfavorable (+17 kJ/mol).

The adsorption of hydrogen over  $Ni_3S_1$ , as shown in Figure 5, part C, demonstrates somewhat different results. Compared to adsorption on the  $Ni_3S_2$  cluster, dissociative adsorption is now favored over molecular adsorption. This reversal in the mode of adsorption can be attributed to the electronic role of the removed sulfur atom (S4). On the basis of BOC and least metal atom sharing principles, one would predict that the extra 2-fold sulfur (S4) in the  $Ni_3S_2$  cluster has a through-metal attractive interaction with the molecularly bound  $H_2$ . Van de Kerkhof et al.<sup>67</sup> demonstrated analogous results for enhanced ammonia adsorption on copper due to the presence of oxygen and a through-metal attractive interaction. The same sulfur atom (S4) acts in a similar manner to weaken the binding of the two 2-fold-bound hydride species which share two metal atoms (one each) with S4. The removal of this sulfur (S4) to form  $Ni_3S_1$  eliminates both the enhanced stabilization for molecular hydrogen and the repulsive

(66) Lide, D. R. *Handbook of Chemistry and Physics*; CRC Press: Boca Raton, FL, 1990; Vol. 71.

(67) Van de Kerkhof, B. J. C. S.; Biemolt, W.; Jansen, A. P. J.; van Santen, R. A. *Surf. Sci.* 1993, 284, 361–371.

Table 3. Computed Binding and Adsorption Energies

reaction	$E_{NLSD}$ (kJ/mol)
Sulfur Addition/Removal Chemistry	
$\text{Ni}_3\text{S}_3 + \text{S} \rightarrow \text{Ni}_3\text{S}_2$	-459
$\text{Ni}_3\text{S}_2 + \text{S} \rightarrow \text{Ni}_3\text{S}_3$	-391
$\text{Ni}_3\text{S}_3 + \text{S} \rightarrow \text{Ni}_3\text{S}_4$	-354
$\text{Ni}_3\text{S}_3 + \text{S} \rightarrow \text{Ni}_4\text{S}_4$	-398
$\text{Ni}_4\text{S}_4 + \text{S} \rightarrow \text{Ni}_4\text{S}_5$	-270
Adsorption Energies	
$\text{Ni}_3\text{S}_1 + \text{H}_2 \rightarrow \text{Ni}_3\text{S}_1-\text{H}_2$	-42.5
$\text{Ni}_3\text{S}_1 + \text{H}_2 \rightarrow \text{Ni}_3\text{S}_1-2\text{H}$ (homo)	-51.5
$\text{Ni}_3\text{S}_1 + \text{H}_2\text{S} \rightarrow \text{Ni}_3\text{S}_1-\text{SH}-\text{H}$ (2-fold)	-185
$\text{Ni}_3\text{S}_2 + \text{H} \rightarrow \text{Ni}_3\text{S}_2-\text{H}$ (1-fold)	-180
$\text{Ni}_3\text{S}_2 + \text{H} \rightarrow \text{Ni}_3\text{S}_2-\text{H}$ (2-fold)	-254
$\text{Ni}_3\text{S}_2 + \text{H} \rightarrow \text{Ni}_3\text{S}_2-\text{H}$ (3-fold)	-203
$\text{Ni}_3\text{S}_2 + \text{H}_2 \rightarrow \text{Ni}_3\text{S}_2-\text{H}_2$	-62
$\text{Ni}_3\text{S}_2 + \text{H}_2 \rightarrow \text{Ni}_3\text{S}_2-2\text{H}$ (homo)	-23
$\text{Ni}_3\text{S}_2 + \text{H}_2 \rightarrow \text{Ni}_3\text{S}_2-\text{SH}-\text{H}$ (hetero)	-31
$\text{Ni}_3\text{S}_2 + \text{H}_2 \rightarrow \text{Ni}_3\text{S}_2-\text{SH}-\text{H}$ (1-fold)	+17
$\text{Ni}_3\text{S}_2 + \text{H}_2\text{S} \rightarrow \text{Ni}_3\text{S}_2-\text{H}_2\text{S}$	-93
$\text{Ni}_3\text{S}_2 + \text{H}_2\text{S} \rightarrow \text{Ni}_3\text{S}_2-\text{SH}-\text{H}$	-73
$\text{Ni}_3\text{S}_2 + \text{Thio} \rightarrow \text{Ni}_3\text{S}_2-\eta^1\text{-Thio}$	-85
$\text{Ni}_3\text{S}_2 + \text{Thio} \rightarrow \text{Ni}_3\text{S}_2-\eta^4\text{-Thio}$	-137
$\text{Ni}_3\text{S}_2 + \text{DHT} \rightarrow \text{Ni}_3\text{S}_2-\eta^1\text{-Thio}$	-120
$\text{Ni}_3\text{S}_2 + \text{DHT} \rightarrow \text{Ni}_3\text{S}_2-\eta^4\text{-Thio}$	-159
$\text{Ni}_3\text{S}_3 + \text{H} \rightarrow \text{Ni}_3\text{S}_3-\text{H}$ (2-fold)	-234
$\text{Ni}_3\text{S}_3 + \text{H}_2 \rightarrow \text{Ni}_3\text{S}_2-\text{SH}-\text{H}$ (2-fold)	+13
Adsorption on $\text{Ni}_4\text{S}_4$	
$\text{Ni}_4\text{S}_4\text{H}_2 \xrightarrow{\text{on single Ni site}} \text{Ni}_4\text{S}_4-\text{H}_2$	nonbonding (>+200)
$\text{Ni}_4\text{S}_4 + \text{H}_2 \xrightarrow{\text{heterolytic smf parallel to Ni-S bond}} \text{Ni}_4\text{S}_3-\text{SH}-\text{H}$	nonbonding (>+200)
$\text{Ni}_4\text{S}_4 + \text{H}_2 \xrightarrow{\text{on two S sites}} \text{Ni}_4\text{S}_2-(\text{SH})_2$	nonbonding (>+200)
$\text{Ni}_4\text{S}_4 + \text{H}_2\text{S} \xrightarrow{\text{S at M-M bridge site}} \text{Ni}_4\text{S}_4-\text{H}_2\text{S}$	nonbonding (>+200)
$\text{Ni}_4\text{S}_4 + \text{Thio} \xrightarrow{\text{S at M-M bridge site (parallel to upper plane)}} \text{Ni}_4\text{S}_4-\text{TH}$	nonbonding (>+200)
$\text{Ni}_4\text{S}_4 + \text{Thio} \xrightarrow{\text{S at M-M bridge site (perpendicular to upper plane)}} \text{Ni}_4\text{S}_4-\text{TH}$	+77

Table 4. Comparison of Bond Energies Estimated for Bulk Sulfides and Computed from DGauss Calculations

bulk estimated bond energy (kJ/mol)	DGauss estimated bond energy (kJ/mol)
Ni-S 116	$\text{Ni}_4\text{S}_4 \rightarrow \text{Ni}_4\text{S}_3 + \text{S}$ 133
	$\text{Ni}_4\text{S}_5 \rightarrow \text{Ni}_4\text{S}_4 + \text{S}$ 135
	$\text{Ni}_3\text{S}_2 \rightarrow \text{Ni}_3\text{S}_1 + \text{S}$ 153
	$\text{Ni}_3\text{S}_3 \rightarrow \text{Ni}_3\text{S}_2 + \text{S}$ 195
	$\text{Ni}_3\text{S}_4 \rightarrow \text{Ni}_3\text{S}_3 + \text{S}$ 177

interactions for dissociatively bound hydrogens. This is portrayed by the trends in adsorption energies for these two systems depicted in Figure 5. Molecular adsorption is diminished from -62 to -42.5 kJ/mol, while the dissociative adsorption increases from -23 to -52 on going from the  $\text{Ni}_3\text{S}_2$  to the  $\text{Ni}_3\text{S}_1$  cluster. The net effect is that dissociative hydrogen adsorption is slightly favored over molecular adsorption on the  $\text{Ni}_3\text{S}_1$  cluster.

A direct orbital or electronic analysis of the bonding of  $\text{H}_2$  on the  $\text{Ni}_3\text{S}_2$  and  $\text{Ni}_3\text{S}_1$  clusters is difficult due to the structural rearrangements which accompany changes in the cluster. The optimized clusters shown in Figure 5, for example, demonstrate a decrease in the Ni-H bond length, yet a weaker adsorption on going from  $\text{Ni}_3\text{S}_2$  to  $\text{Ni}_3\text{S}_1$ . Somewhat hidden in this is the fact that the H-H bond has elongated. This requires energy and thus weakens the adsorption on  $\text{Ni}_3\text{S}_1$ . In an effort to probe the initial electronic features which control adsorption, the optimized  $\text{H}_2-\text{Ni}_3\text{S}_2$  cluster was compared with an  $\text{H}_2-\text{Ni}_3\text{S}_1$  cluster which was cut directly from the  $\text{H}_2-\text{Ni}_3\text{S}_2$  cluster (i.e. the bridging sulfur,

S6, from  $\text{H}_2-\text{Ni}_3\text{S}_2$  was removed). The geometry of this cluster was not allowed to optimize, thus enabling comparison with the  $\text{H}_2$  on  $\text{Ni}_3\text{S}_2$ . The results indicate that both the one-electron and nuclear-electron repulsion energy increase by over 12 hartree when going from  $\text{H}_2$  on  $\text{Ni}_3\text{S}_2$  to  $\text{H}_2$  on  $\text{Ni}_3\text{S}_1$ . While most of this is offset by an increase in the orbital overlap interactions, the net effect is still a more favorable bonding of molecular  $\text{H}_2$  on the  $\text{Ni}_3\text{S}_2$  cluster. This also shows up in the decreased Ni-Ni and increased Ni-H bond orders on going from  $\text{Ni}_3\text{S}_1$  to  $\text{Ni}_3\text{S}_2$ . A short summary of the  $\text{H}_2$  antibonding orbitals, depicted in Figure 6, indicates that two  $\text{H}_2$  antibonding orbitals which are unoccupied on the  $\text{Ni}_3\text{S}_2$  cluster (-0.81 and -2.237 eV on  $\text{Ni}_3\text{S}_2$ ) are considerably lowered in energy (-5.24 and -6.108 eV) on going to the  $\text{Ni}_3\text{S}_1$  cluster. These orbitals now become occupied, which is a direct indication that the  $\text{H}_2$  bond will stretch (and may even dissociate) over  $\text{Ni}_3\text{S}_1$ . When the structure is allowed to optimize (Figure 5C), there is indeed a stretch in the H-H bond. These results are consistent with the findings of Seigbahn, Blomberg, and Bauschlicher<sup>59</sup> for  $\text{H}_2$  dissociation on model Ni(100) clusters. They attribute  $\text{H}_2$  dissociation to the donation of electrons from the Ni surface into the  $\text{H}_2$  antibonding orbital. The weak H-H bond translates into a stronger Ni-H bond.

The results for the adsorption of hydrogen sulfide on  $\text{Ni}_3\text{S}_1$  and  $\text{Ni}_3\text{S}_2$  clusters are depicted in Figure 7. The optimized structures and their associated adsorption energies indicate that both molecular and dissociative adsorption are feasible. Similar to the results for hydrogen, molecular adsorption of  $\text{H}_2\text{S}$  (-93 kJ/mol) on  $\text{Ni}_3\text{S}_2$  is favored over dissociative addition (-73 kJ/mol).

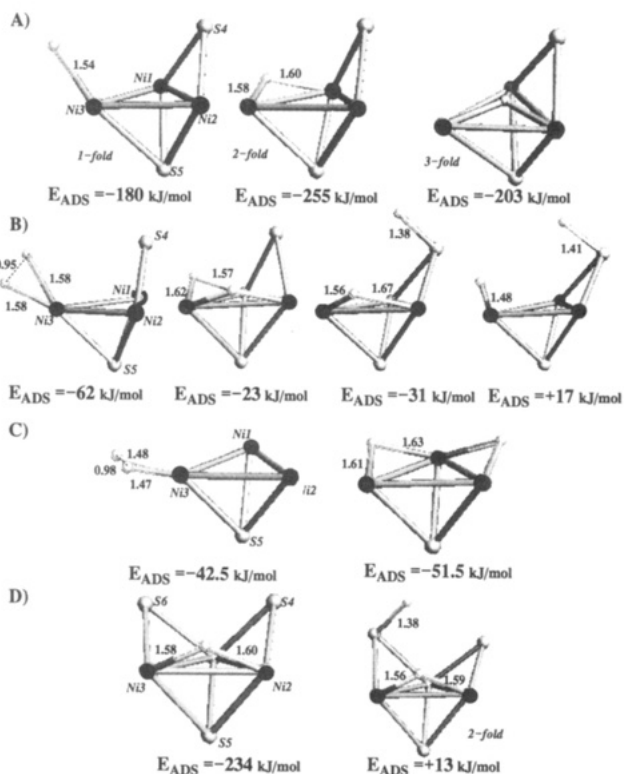


**Figure 5.** Adsorption of (A) atomic hydrogen on Ni<sub>3</sub>S<sub>2</sub>, (B) H<sub>2</sub> on Ni<sub>3</sub>S<sub>2</sub>, (C) H<sub>2</sub> on Ni<sub>3</sub>S<sub>1</sub>, and (D) atomic hydrogen on Ni<sub>3</sub>S<sub>3</sub>.

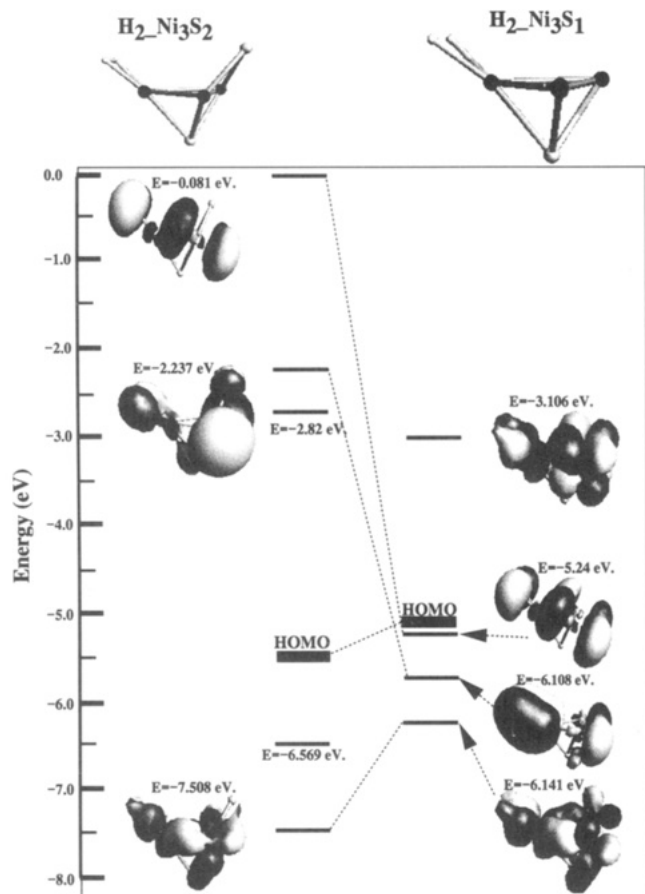


**Figure 6.** Frontier orbitals with substantial H<sub>2</sub> antibonding character in the adsorption of hydrogen on Ni<sub>3</sub>S<sub>2</sub> and Ni<sub>3</sub>S<sub>1</sub>. The underlying geometry for both H<sub>2</sub>-Ni<sub>3</sub>S<sub>2</sub> and H<sub>2</sub>-Ni<sub>3</sub>S<sub>1</sub> clusters are depicted at the top of the page.

mol). However, on the Ni<sub>3</sub>S<sub>1</sub> cluster, as was the case for hydrogen, the repulsive interactions derived from the sharing of metal atoms

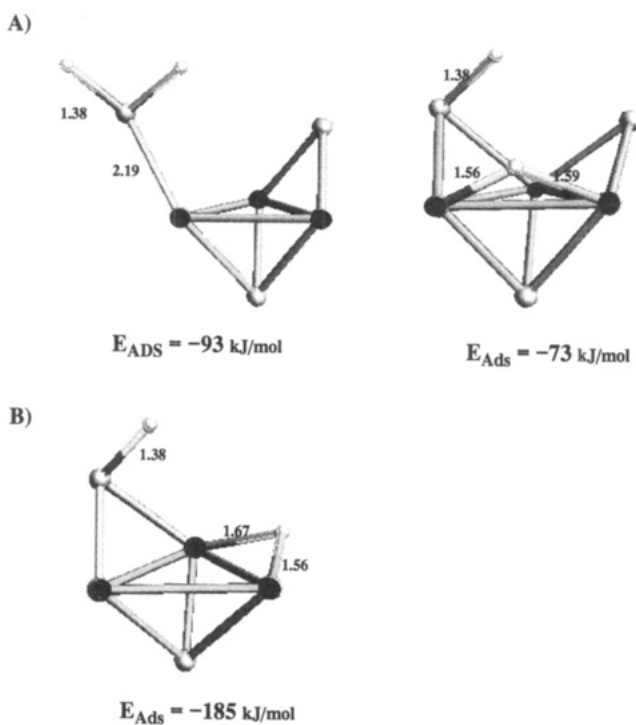


**Figure 7.** Adsorption of hydrogen sulfide on Ni<sub>3</sub>S<sub>x</sub> clusters: (A) molecular and dissociative adsorption of H<sub>2</sub>S over Ni<sub>3</sub>S<sub>2</sub> and (B) dissociative adsorption of H<sub>2</sub>S over Ni<sub>3</sub>S<sub>3</sub>.

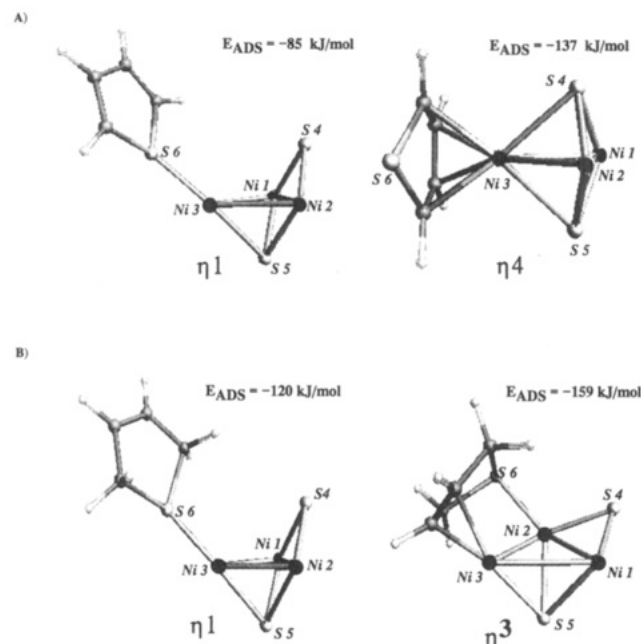


**Figure 8.** Adsorption of thiophene and 2,5-dihydrothiophene on Ni<sub>3</sub>S<sub>x</sub>: (A) adsorption of thiophene in  $\eta^1$  and  $\eta^4$  configurations and (B) adsorption of 2,5-dihydrothiophene in  $\eta^1$  and  $\eta^3$  configurations.

are reduced. The dissociative adsorption to produce 2-fold-bound SH and H fragments now becomes much more favorable (-185 kJ/mol).

As was discussed earlier, over seven different modes for thiophene adsorption have been presented in the literature. We explored four different configurations:  $\eta^1-\mu^2$  (coordinated to two nickel atoms),  $\eta^1-\mu^1$  (coordinated to a single nickel atom),  $\eta^5$  bound, and  $\eta^4$  bound. Both the  $\eta^1-\mu^2$ - and  $\eta^5$ -bound structures were chosen as initial starting geometries. Their optimized structural outcomes were the  $\eta^1-\mu^1$  and  $\eta^4$ -bound configurations depicted Figure 8, part A.

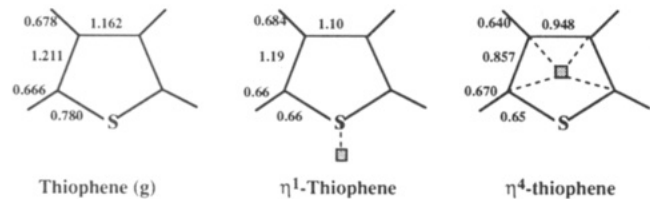
The  $\eta^4$  mode was the most favorable configuration with an adsorption energy of -137 kJ/mol, whereby there is a direct

interaction between the d orbitals on the metal and the  $\pi$  system of the thiophene. Comparing the  $\eta^4$  with the initial  $\eta^5$  configuration, we note that the sulfur atom on the thiophene is bent slightly out of the molecular plane. The results for  $\eta^1$  adsorption indicate that thiophene prefers to sit with the sulfur bound to the 1-fold coordination site rather than the 2-fold coordination site, which was favored for atomic sulfur. The energy for adsorption at the 1-fold site was  $-85$  kJ/mol. This is some  $50$  kJ/mol less favorable than the  $\eta^4$  adsorption.

A closer analysis of the literature indicates that at low coverages,<sup>13</sup> i.e., highly unsaturated environments, thiophene prefers to sit parallel to the surface. Either  $\eta^5$  or  $\eta^4$  bonding modes might be likely cluster analogs to this situation, whereby there is an enhanced stabilization due to  $\pi$  bonding. This explains the more favorable binding for  $\eta^4$  adsorption of thiophene on the  $\text{Ni}_3\text{S}_2$  cluster. However, under conditions of higher coverage where each metal atom is near coordinatively saturated, thiophene prefers to sit perpendicular or tilted to the surface.<sup>13</sup> We expect that the  $\eta^1$  configuration will become the preferred adsorption mode and that thiophene will bind via  $\eta^1$  adsorption on our more saturated  $\text{Ni}_3\text{S}_3$  or  $\text{Ni}_3\text{S}_4$  clusters. As we demonstrate in the next section, coadsorption of hydrogen to the  $\text{Ni}_3\text{S}_2$  cluster shifts the preference of thiophene adsorption from  $\eta^4$  to  $\eta^1$  coordination.

Zonneville et al.<sup>40</sup> make the interesting point that the most strongly adsorbed configuration is not necessarily the one which carries out the chemistry. Their results show that thiophene was more tightly bound at the  $\eta^1$  site rather than at the  $\eta^5$  site. However, they report that the  $\eta^5$  is more active for desulfurization due to the enhanced weakening of the carbon–sulfur bond, as is demonstrated by the increase in population of the antibonding 3b1 molecular orbital of thiophene and the decrease of the S–C bond order.

We performed a similar analysis to test for the weakening of the carbon–sulfur bond in our clusters for various configurations. The bond orbital overlap populations for the carbon–sulfur, carbon–carbon, and carbon–hydrogen bonds are presented here for the free thiophene and  $\eta^1$ - and  $\eta^4$ -bound thiophene complexes.



These results demonstrate that there is a small weakening of the carbon–sulfur bond as one moves to higher coordination. A somewhat more substantial increase in the C–S antibonding population would be expected if the thiophene adsorbed in the  $\eta^5$  configuration, as was proposed by Zonneville, due to the direct interaction of both the carbon and sulfur with the exposed nickel site.

The differences for the most favorable *adsorption* site as predicted by Zonneville ( $\eta^1$ ) and those reported here ( $\eta^4$ ) are most likely due to differences in the coordination at the metal atom centers. In fact, Zonneville demonstrated that as the metal atom becomes increasingly unsaturated, the  $\eta^5$  binding increases significantly. This is more consistent with our findings and those shown experimentally.

The hydrogenated thiophene intermediate, 2,5-dihydrothiophene (DHT), is a relatively stable surface species and has been cited as an important precursor for the carbon–sulfur bond scission reaction.<sup>13,26–28,68</sup> We examined the adsorption of 2,5-dihydrothiophene in both  $\eta^1$  and  $\eta^3$  binding configurations, which are the subsequent results from the initial  $\eta^1$  and  $\eta^4$  binding modes of the parent thiophene. The optimized adsorbate–cluster

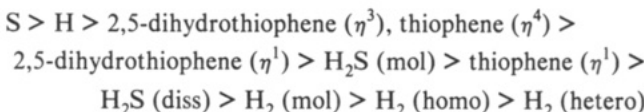
geometries for these two modes and their associated adsorption energies are depicted in part B of Figure 8. 2,5-Dihydrothiophene is strongly adsorbed in each of these two modes,  $-122$  and  $-160$  kJ/mol for  $\eta^1$  and  $\eta^3$ , respectively.

The optimized structural configuration of the  $\eta^3$ -bound DHT on  $\text{Ni}_3\text{S}_2$ , depicted in part B of Figure 8, bears an interesting resemblance to the 2,5-dihydrothiophene  $\eta^4\text{-}\mu^3\text{-Ru}_3(\text{CO})_9$  adsorption complex determined by X-ray crystallography and reported by Choi, Daniels, and Angelici.<sup>69</sup> Both structures feature a strong ethylene-like bond to a vacant Ni atom, coordinative bonding of the remaining carbons with the transition metal framework, and sulfur binding at an adjacent Ni1 atom site. The main difference between the two regards the metal coordination site. In Angelici's structure, the CO ligands are quite flexible and arranged such that DHT binds to the 3-fold metal site ( $\mu^3$ ). In our cluster, however, the repulsive interactions of the adjacent sulfur atom (S4) force DHT to sit at the 2-fold coordination site ( $\mu^2$ ).

The  $\eta^1$  and  $\eta^3$  binding of DHT appear to be somewhat stronger than the binding of the parent thiophene at  $\eta^1$  and  $\eta^4$  sites. The lone pair of electrons associated with the sulfur in thiophene are delocalized about the ring. In the saturated forms (dihydro- and tetrahydrothiophene), however, the electron pair is more tightly localized *on* the sulfur. This enhances the basicity of the sulfur and works to increase the  $\sigma$ -bonding interaction with the Ni cation site. In the  $\eta^3$  mode of adsorption, the DHT has an additional enhancement due to the stabilization of utilizing two coordinatively unsaturated Ni atom binding sites.

In general, the adsorption results on the  $\text{Ni}_3\text{S}_2$  cluster presented in Figures 5, 7, and 8 demonstrate that structural reorganization of the cluster is an important element in determining adsorbate binding. In most of these examples, one of the 3-fold-bound sulfur atoms (S4) must first migrate to a 2-fold bridge site, in order to accommodate the incoming adsorbate. Molecular substrates prefer the 1-fold nickel atom site which is directly across from, yet not involved in, the new Ni–S–Ni bridge. Adatoms and radical fragments, however, prefer higher coordination sites and tend to induce structural rearrangements to reduce the number of shared metal atoms. These results can be rationalized along the lines of the principle of least metal atom sharing.

Trends in the adsorption energetics are clearly dependent upon the cluster Ni/S ratio, or more formally the oxidation state. The adsorption on  $\text{Ni}_3\text{S}_2$  demonstrates the following order:



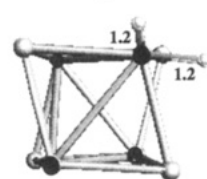
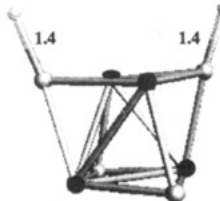
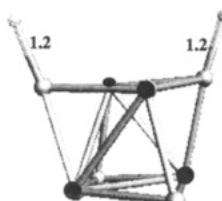
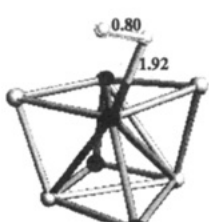
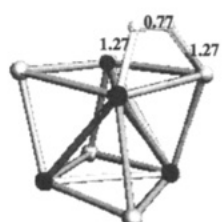
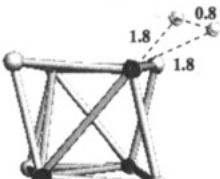
This order, however, changes to



for the adsorption of small adsorbates on the  $\text{Ni}_3\text{S}_1$  cluster.

The chemistry of the  $\text{Ni}_4\text{S}_4$  complex was found to be much less interesting than the chemistry of the  $\text{Ni}_3\text{S}_2$  complex. This complex was basically inactive toward all of the molecular adsorbates studied. Figure 9 depicts the starting geometries for the  $\text{H}_2$  interaction with this cluster and the resulting intermediate complexes formed after 8–10 iterations in the optimization cycle. In part A, hydrogen was homolytically dissociated over a single Ni atom site. The energy of this system monotonically decreased as the Ni–H distance was increased. The intermediate structure shown on the right-hand side of this figure clearly indicates that both hydrogen atoms are moving away from the cluster toward the gas phase to form molecular hydrogen that is removed from

(69) Choi, M. G.; Daniels, L. M.; Angelici, R. J. *Inorg. Chem.* 1991, 30, 3647–3651.

**Initial Adsorption Geometry****Intermediate Optimized Geometry****Figure 9.** Attempted adsorption of H<sub>2</sub> on Ni<sub>4</sub>S<sub>4</sub>.

the cluster. The overall energy for this step is large and positive, thus indicating that adsorption via this mode is improbable. In part B, the molecular axis (bond) of hydrogen is placed parallel to one of the Ni–S bonds and stretched by about 0.3 Å to help initiate heterolytic dissociation. The optimized intermediate structure which is shown on the central RHS of Figure 9 also indicates that the hydrogen prefers its gas-phase molecular geometry far removed from the cluster. The large positive adsorption energy supports the idea that molecular hydrogen does not undergo heterolytic dissociation. The final starting complex was chosen such that the hydrogens were now completely dissociated and attached to neighboring sulfurs to form two SH moieties, as is depicted in part C of Figure 9. While the hydrogens remained attached to the cluster throughout the optimization, the energetics suggest that this form of adsorption is also unfavorable. The inability to dissociate hydrogen over the Ni<sub>4</sub>S<sub>4</sub> cubane compares quite well with the experimental findings of Curtis,<sup>70</sup> who demonstrated that hydrogen would not dissociate over Cp'<sub>2</sub>Mo<sub>2</sub>Co<sub>2</sub>(CO)<sub>2</sub>S<sub>4</sub> or Cp'<sub>2</sub>Mo<sub>2</sub>Co<sub>2</sub>(CO)<sub>4</sub>S<sub>3</sub> cubane clusters, even at high temperatures and H<sub>2</sub> partial pressures. A similar evaluation of the adsorption of H<sub>2</sub>S and thiophene on the Ni<sub>4</sub>S<sub>4</sub> cluster demonstrated that these species were also inactive to adsorption. Clearly, the chemistry over this cluster is limited.

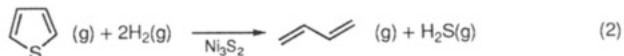
Interestingly, Welters et al.<sup>7</sup> found a maximum activity for thiophene HDS to occur for Ni/S ratios of 3/2. This qualitatively matches our results, where the Ni<sub>3</sub>S<sub>2</sub> cluster, which has a Ni/S ratio of 3/2, was much more active toward adsorption than the Ni<sub>4</sub>S<sub>4</sub> cluster, which has a ratio of 1.

**III. Role of Preadsorbed Precursors.** While the intrinsic adsorption energies presented in Figures 5 and 7–9 provide a substantial start in the analysis of the overall reaction pathways, they are devoid of any through-cluster adsorbate–adsorbate interaction effects. In this section we evaluate the magnitude of the thiophene–hydrogen interactions. In the first part of Table 5, the effect of preadsorbed hydrogen on the adsorption of thiophene is summarized. In the thiophene  $\eta^1$  mode, preadsorbed hydrogen (on adjacent 2-fold metal atom coordination sites)

reduces the adsorption energy from –85 to –74 kJ/mol, a change of +11 kJ/mol. In the  $\eta^4$  configuration, however, the role of preadsorbed hydrogen is much stronger and reduces the adsorption from –137 to –66 kJ/mol, a 71 kJ/mol difference. Interestingly, the adsorption of thiophene  $\eta^1$  now becomes slightly favored over the  $\eta^4$  mode. The repulsive interactions responsible for the lowering of the adsorption energy are due to the higher coordination at the metal atom binding site and can be explained in terms of the principle of least metal atom sharing.<sup>52,71</sup> The  $\eta^4$  mode is affected to a much greater extent due to its increased number of metal–adsorbate bonds.

As to be expected, an analogous set of results were found for the effect of preadsorbed thiophene on hydrogen adsorption. For  $\eta^1$ -adsorbed thiophene, hydrogen adsorption is lowered from –23 to –14 kJ/mol, while that for  $\eta^4$  was changed to +47 kJ/mol.

**IV. Reaction Path Analysis.** The quantitative adsorption energetics computed in this work made it possible to analyze the energetics for various reaction pathways and their likelihood as possible catalytic HDS cycles for the overall conversion of thiophene to butadiene and hydrogen sulfide (eq 2). We examined



four specific cases. The first two consider thiophene adsorbed  $\eta^1$  as the predominant precursor for hydrodesulfurization. The third case presumes that the  $\eta^4$  adsorption of thiophene dominates. In each of these three paths, sulfur addition to the cluster is regarded as the preliminary step to desulfurization. In the final pathway examined, sulfur removal from the cluster to form a vacant site is regarded as the initial step in the HDS mechanism. Each of these cycles assumes that the hydrogenation to the dihydrothiophene intermediate is followed by carbon–sulfur bond scission rather than hydrogenation to the tetrahydrothiophene intermediate. While the kinetics for this subsequent hydrogenation step is of interest, the electronic and energetic factors governing adsorption and dissociation of THT are likely to be quite similar to those of DHT.

The results for the  $\eta^1$ -thiophene adsorption initiated cycle are presented in Figure 10. The intermediates involved in each step of the catalytic cycle are depicted in part A: (1)  $\eta^1$  adsorption of thiophene, (2) dissociative addition of hydrogen, (3) hydrogenation of thiophene to 2,5-dihydrothiophene, (4) C–S bond homolysis, (5) adsorption of H<sub>2</sub> over Ni<sub>3</sub>S<sub>2</sub>, and (6) removal of hydrogen sulfide. Each step in Figure 10A displays the optimized intermediates. The corresponding reaction energies accompanying each step,  $\Delta E_j$ , are defined by eq 3:

$$\Delta E_j = \sum_{i=1}^{N_{\text{comp}}} \nu_{ij} E_i \quad (3)$$

where  $j$  refers to the particular reaction step,  $i$  to the components or intermediates,  $E_i$  the nonlocally corrected total energies for component  $i$ , and  $\nu_{ij}$  their stoichiometric coefficient (for component  $i$  in reaction  $j$ ). The computed values for each of these six steps are displayed in the potential energy diagram for the overall cycle in part B of Figure 10. The overall reaction energy for this cycle is –23 kJ/mol and agrees quite well with the –27 kJ/mol (the dotted horizontal line) predicted from a thermochemical analysis. Both carbon–sulfur bond homolysis and sulfur removal are recognized as the two most endothermic steps in the process. Their overall energetic values of +70 and +73 are quite similar. Both of these steps have also been cited in the literature as possible rate-limiting steps.

The relative ordering of the initial adsorption steps was analyzed by allowing hydrogen adsorption to precede the  $\eta^1$  adsorption of

(70) Riaz, U.; Curnow, O.; Curtis, D. M. *J. Am. Chem. Soc.* 1991, 113, 1416.

(71) Van Santen, R. A. *Theoretical Heterogeneous Catalysis*; World Scientific Publishing Co. Pte. Ltd., Singapore, 1991; Vol. 5.

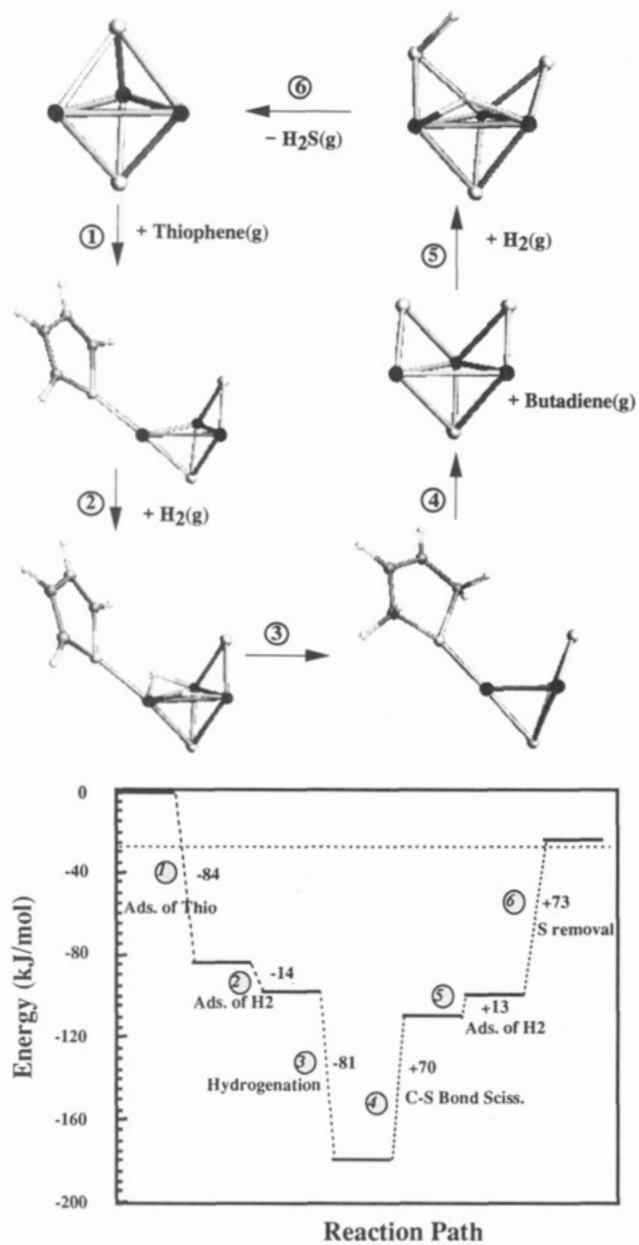


**Figure 10.** Proposed catalytic HDS cycle 1 for the  $\eta^1$ -adsorbed thiophene and 2,5-dihydrothiophene intermediates on  $\text{Ni}_3\text{S}_2$  (thiophene adsorption initiated): (A) optimized structures for each step of the catalytic reaction path and (B) corresponding energies for each step.

thiophene. The resulting catalytic cycle for the hydrogen adsorption mediated cycle is presented in Figure 11. Recall that, for the adsorption of hydrogen on the  $\text{Ni}_3\text{S}_2$  cluster, surface reconstruction takes place to accommodate and stabilize molecular hydrogen. This is the first step in Figure 11. Subsequent dissociation of molecular hydrogen (step 2) is required to form the dihydriyl- $\text{Ni}_3\text{S}_2$  complex and costs +38 kJ/mol in energy. Thiophene adsorption is slightly less favorable in this cycle (-74 kJ/mol rather than -84 kJ/mol) due to the competition (repulsion) with the hydriyl groups for the metal center. The remainder of this cycle is identical to that shown in Figure 10. Neither the C-S bond scission nor sulfur removal via the recombinative SH and H desorption to gaseous  $\text{H}_2\text{S}$  are affected by the ordering of the initial adsorption steps.

The third reaction path, which is depicted in Figure 12, involves a change in the binding configuration of thiophene and its subsequent intermediates. Cycles 1 and 2 were based on the  $\eta^1$  adsorption of thiophene. In this cycle, thiophene is adsorbed in the more stable  $\eta^4$  arrangement (-137 kJ/mol). This is followed by the heterolytic dissociative addition of hydrogen, which is

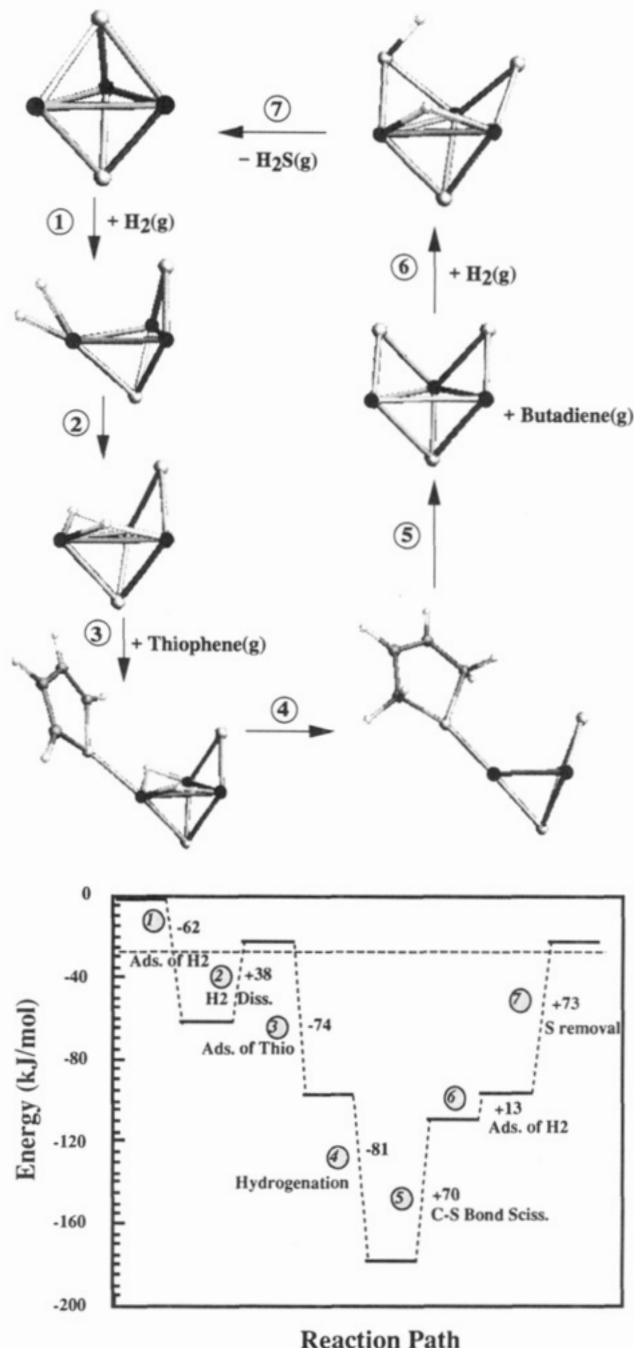


**Figure 11.** Proposed catalytic HDS cycle 2 for the  $\eta^1$ -adsorbed thiophene and 2,5-dihydrothiophene intermediates on  $\text{Ni}_3\text{S}_2$  ( $\text{H}_2$  adsorption initiated): (A) optimized structures for each step of the catalytic reaction path and (B) corresponding energies for each step.

slightly endothermic at +10 kJ/mol. The homolytic dissociative addition of  $\text{H}_2$  at this site was found to be highly unfavorable due to the considerable number of metal ligand interactions (see Table 5). Therefore, heterolytic dissociative addition was the only available route (+11 kJ/mol). The subsequent hydrogenation of thiophene yields an  $\eta^3$ -bound 2,5-dihydrothiophene. The strong  $\eta^3$  interaction serves to enhance the overall reaction energy for hydrogenation, which was -81 kJ/mol for hydrogenation of  $\eta^1$ -thiophene to  $\eta^1$ -dihydrothiophene and is now -92 kJ/mol. In addition, the carbon-sulfur bond scission step is increased by +37 kJ/mol (from +70 to +107 kJ/mol) with respect to the gas phase. Once again the two most endothermic steps appear to be C-S bond scission and sulfur removal.

The final cycle considered mimics the established notion for bulk metal sulfides that sulfur removal is a prerequisite to HDS chemistry. Both the overall cycle and reaction path diagram are

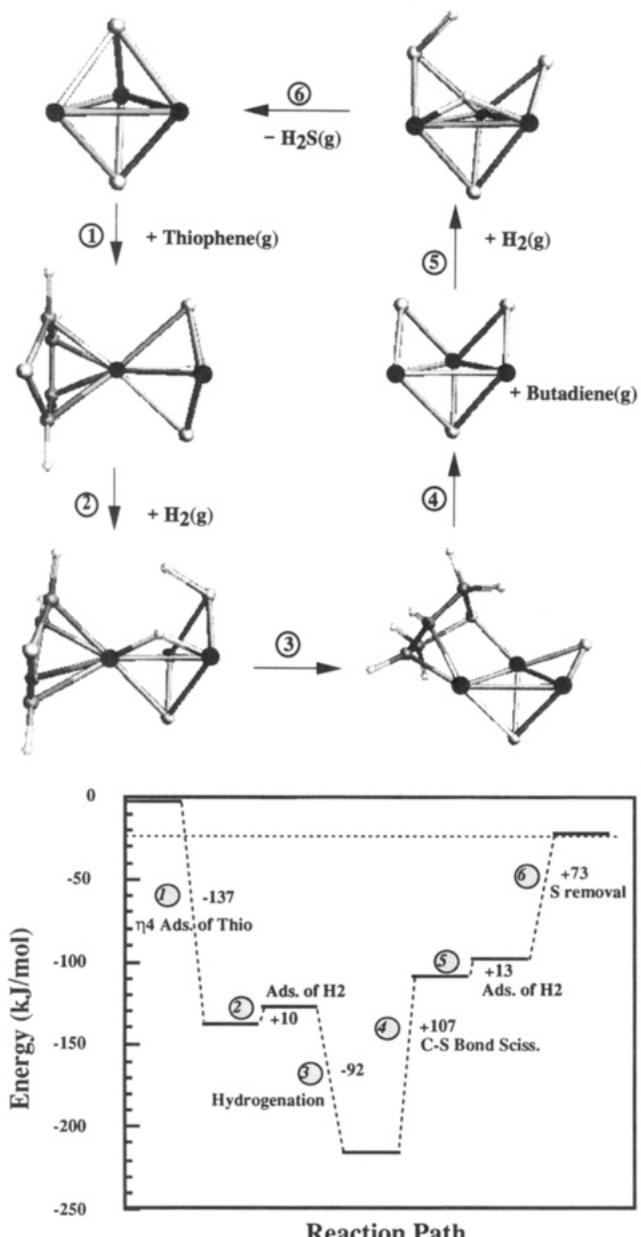


**Figure 12.** Proposed catalytic HDS cycle 3 for the  $\eta^4$ -adsorbed thiophene and  $\eta^3$ -2,5-dihydrothiophene intermediates on  $\text{Ni}_3\text{S}_2$ : (A) optimized structures for each step of the catalytic reaction path and (B) corresponding energies for each step.

**Table 5.** Effects of Preadsorbed Hydrogen on Thiophene Adsorption and Preadsorbed Thiophene on Hydrogen Adsorption on the  $\text{Ni}_3\text{S}_2$  Cluster

reaction	energy (kJ/mol)
<b>Effects of Preadsorbed Hydrogen</b>	
η <sup>1</sup> -adsorption	
$\text{Ni}_3\text{S}_2 + \text{thiophene(g)} \rightarrow \text{Ni}_3\text{S}_2-\eta^1\text{-Thio}$	-85
$\text{Ni}_3\text{S}_2-2\text{H} + \text{thiophene(g)} \rightarrow \text{Ni}_3\text{S}_2-2\text{H}-\eta^1\text{-Thio}$	-74
η <sup>4</sup> -adsorption	
$\text{Ni}_3\text{S}_2 + \text{thiophene(g)} \rightarrow \text{Ni}_3\text{S}_2-\eta^4\text{-Thio}$	-137
$\text{Ni}_3\text{S}_2-2\text{H} + \text{thiophene(g)} \rightarrow \text{Ni}_3\text{S}_2-2\text{H}-\eta^4\text{-Thio}$	-66
<b>Effects of Preadsorbed Thiophene</b>	
η <sup>1</sup> -adsorption	
$\text{Ni}_3\text{S}_2 + \text{H}_2\text{(g)} \rightarrow \text{Ni}_3\text{S}_2-2\text{H}$	-23
$\text{Ni}_3\text{S}_2-\eta^1\text{-Thio} + \text{H}_2\text{(g)} \rightarrow \text{Ni}_3\text{S}_2-\eta^1\text{-Thio}-2\text{H}$	-14
η <sup>4</sup> -adsorption	
$\text{Ni}_3\text{S}_2 + \text{H}_2\text{(g)} \rightarrow \text{Ni}_3\text{S}_2-2\text{H}$	-23
$\text{Ni}_3\text{S}_2-\eta^4\text{-Thio} + \text{H}_2\text{(g)} \rightarrow \text{Ni}_3\text{S}_2-\eta^4\text{-Thio}-2\text{H}$	+47

shown in Figure 13. These results indicate that this path is least favored over all of those studied due to the prohibitively large

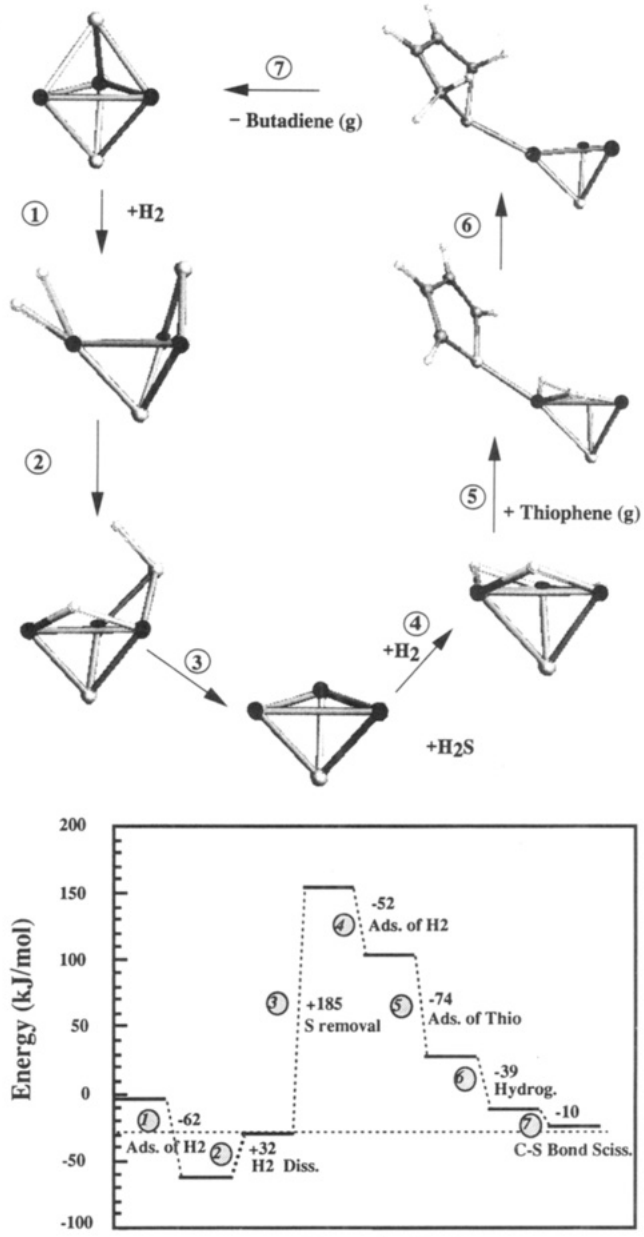


**Figure 13.** Proposed catalytic HDS cycle 4 initiated by sulfur removal from the  $\text{Ni}_3\text{S}_2$  cluster: (A) optimized structures for each step of the catalytic reaction path and (B) corresponding energies for each step.

endoothermic sulfur removal step (+185 kJ/mol). This scheme may be more preferable for the bulk NiS systems and even for some of the sulfur-rich clusters described here ( $\text{Ni}_4\text{S}_5$ ,  $\text{Ni}_4\text{S}_4$ , and  $\text{Ni}_3\text{S}_3$ ), whereby the cost of sulfur removal would be less. However, the severe energy cost makes this an unlikely path for HDS over  $\text{Ni}_3\text{S}_2$ .

While all the energies reported in Figures 10–13 are based on overall reaction enthalpies, we are currently computing detailed reaction coordinates and activation energies for each of these steps. The results of the carbon–sulfur bond scission path which will be reported in a forthcoming communication indicate that ring opening to form the butadiene occurs via a chelotropic Diels–Alder type mechanism. The activated state over different nickel sulfide clusters indicates that the path is controlled by a change in multiplicity from a singlet to a triplet state.

Notwithstanding the absence of these predicted activation energies, the reaction energy schemes presented here provide some general kinetic insights. When one starts with the situation of preadsorbed thiophene, the hydrogenation step to 2,5-dihy-

drothiophene is thermodynamically favorable, whereas the subsequent step of carbon–sulfur bond scission is highly endothermic. The strength of the carbon–sulfur bond then is an important parameter. The single-crystal experiments of Friend<sup>13,28,72</sup> and Gellman and Somorjai<sup>29</sup> are interesting examples of this situation, whereby thiophene is initially adsorbed to the surface. They are essentially transient experiments performed at low partial pressures and on the basis of our analysis should be controlled by carbon–sulfur bond scission. This is consistent with their experimental findings.

Additionally, it is interesting to analyze two different steady-state situations. In the first scenario, the steady-state surface coverage is low. The overall reaction rate then is first order in thiophene, which is consistent with many of the experimental findings over traditional HDS catalysts at low partial pressures.<sup>73,74</sup> The apparent activation barrier for this scheme is essentially measured with respect to the gas phase and therefore is a strong function of both the intrinsic rate constant for either carbon–sulfur bond scission or metal–sulfur cleavage (depending on the rate-determining step) and the equilibrium adsorption constants. If the *intrinsic* activation energies for carbon–sulfur and metal–sulfur bond cleavage follow their thermodynamic reaction energies, which suggest that the two are quite similar, then the *apparent* activation energy, which includes equilibria energetics, is controlled by the sulfur removal step. This is consistent with Norskov's proposal<sup>21</sup> that the most active desulfurization catalyst contains the weakest metal–sulfur interaction energy. However, we cannot exclude a change in the rate-limiting step for clusters which have weaker metal–sulfur bond energies than NiS, which is more consistent with the views of Chianelli and Harris. In addition, we would expect the subsequent saturation of DHT to THT to occur quite readily.

The second steady-state scenario we consider is that for high coverages of sulfur-containing reactive intermediates. Under these conditions, the overall reaction order is zero or negative in thiophene, and the kinetics are now measured with respect to the adsorbed state. This is not a strict function of the equilibria adsorption constants. The rates of carbon–sulfur bond scission and the recombinative removal of H<sub>2</sub>S directly compete. If we assume that the *overall reaction enthalpies* for C–S splitting and sulfur removal represent a significant portion of the real activation barriers for these steps, then the values reported in Figure 10 (70 kJ/mol for C–S scission and 73 kJ/mol for sulfur removal) are consistent with the experimental activation energies reported by Ledoux,<sup>9</sup> which range from 69 to 98 kJ/mol for HDS over small metal sulfide clusters.

### Summary and Conclusions

In general, we have demonstrated that detailed density functional calculations can provide a wealth of valuable information on the binding, adsorption, reaction pathways, and mechanisms involved in the chemistry of hydrodesulfurization over small transition metal sulfide particles.

Calculations on the structure and electronic and energetic configuration of Ni<sub>3</sub>S<sub>y</sub> ( $y = 1\text{--}4$ ) and Ni<sub>4</sub>S<sub>y</sub> ( $y = 3\text{--}5$ ) clusters conclude that atomic sulfur prefers to bind at high coordination sites, e.g. the coordinatively unsaturated 3-fold site, when

(72) Wiegand, B. C.; Uvdal, P.; Friend, C. M. *Surf. Sci.* 1992, 279, 105–112.

(73) Satterfield, C. N.; Roberts, G. W. *AIChE J.* 1960, 14, 159.

(74) Vrinat, M. L. *Appl. Catal.* 1983, 6, 137–158.

(75) Hunzinaga, S.; Klobukowski, M.; Sakai, Y. *J. Phys. Chem.* 1984, 88, 4880.

available. In their absence surface reconstruction can take place to minimize the sharing of metal atom centers and hence lower the binding energy. The addition of sulfur to all clusters studied was a highly exothermic process. Consequently, the removal of sulfur is very endothermic. Binding energies appear to increase with increases in the formal oxidation state of Ni in the cluster.

Adsorption on the Ni<sub>3</sub>S<sub>y</sub> series of clusters is a favorable process on both Ni<sub>3</sub>S<sub>1</sub> and Ni<sub>3</sub>S<sub>2</sub> clusters. Lower Ni/S ratio clusters, however, are much more inactive toward adsorbates. Molecular adsorbates tended to prefer 1-fold coordination sites, whereas dissociated fragments preferred higher 2-fold coordination sites. Molecular adsorption of hydrogen and hydrogen sulfide is favored on the Ni<sub>3</sub>S<sub>2</sub> clusters whereby they are stabilized via a through-metal interaction with a neighboring 2-fold-bound sulfur. These same adsorbates are found to adsorb dissociatively on Ni<sub>3</sub>S<sub>1</sub> whereby the stabilization due to sulfur is removed. Hydrogen binds favorably to both bridge metal atom sites and vacant sulfur atoms. The preference for homolytic and heterolytic dissociation to form hydrol and sulphydrol groups is, therefore, quite similar and a complex function of the cluster structure.

The bond between an adsorbate and a nickel atom binding site is weakened in the presence of additional adsorbates at the same site due to repulsive interactions. However, two adsorbates which bind at *adjacent* nickel atom centers strengthen the binding of one another due to through-metal attractive interactions. This agrees with the principles of bond order conservation and least metal atom sharing.

Thiophene adsorption is favorable in both the  $\eta^1$  and  $\eta^4$  configurations on the Ni<sub>3</sub>S<sub>2</sub> cluster.  $\eta^4$  is the more stable of the two on this cluster, which is due to an increased number of bonds and favorable  $\pi$ -interaction with the coordinatively unsaturated Ni site. At higher sulfur coverages, however, it is speculated that  $\eta^1$  will become the dominant mode for adsorption.

Finally, reaction path analysis leads to two important findings. The first demonstrates that the mechanism proceeds via the initial addition of sulfur-containing adsorbates rather than the initial removal of sulfur from the cluster to form a vacant site. On the basis of known bulk transition metal–sulfur binding energies, this may have been expected and therefore provides a nice consistency check for the calculations. The second point illustrates that under steady-state conditions both carbon–sulfur bond scission and sulfur removal can compete as rate-controlling steps. The resolution of which of these controls the overall kinetics is highly dependent upon reaction conditions.

**Acknowledgment.** We would like to thank Dr. A. P. J. Jansen, Dr. San de Beer, Wim Welters, and Wim Biemolt from the Eindhoven University of Technology and Professor E. J. Baerends from the Free University of Amsterdam for their invaluable technical input. We thank T. Ziegler (Calgary) and D. A. Dixon (DuPont) for their helpful comments. This work was supported by the Dutch Science Foundation (Stimulus project) and the Eindhoven University of Technology. We also wish to acknowledge the computational resources made which were allocated from the National Computing Facilities (NCF) Foundation under project SC-183.

**Supplementary Material Available:** Basis sets, fit sets, and convergence criterion used in the calculations and the overall algorithm (5 pages). This material is contained in many libraries on microfiche, immediately follows this article in the microfilm version of the journal, and can be ordered from the ACS; see any current masthead page for ordering information.